

(12) LEVEL *II*

AD-E900060

NWC TP 6193

AD A 097474

Dynamic Burning Effects in the Combustion of Solid Propellants With Cracks, and the Use of Granular Bed Combustion Models

by
Kenneth K. Kuo
and
Mridul Kumar
Systems Associates
Pennsylvania State University

New

for the

Research Department

DTIC
ELECTE
APR 8 1981
S D B

DECEMBER 1980

NAVAL WEAPONS CENTER
CHINA LAKE, CALIFORNIA 93555



Approved for public release; distribution unlimited

DTIC FILE COPY

4/2 277

81 4 3 002

Naval Weapons Center

AN ACTIVITY OF THE NAVAL MATERIAL COMMAND

FOREWORD

This is the final report for a research program conducted by Systems Associates, Pennsylvania State University, in support of the Aerothermochemistry Division's studies of High Energy Propellant Safety. This facsimile report is reproduced in the original format and has been prepared as a means of disseminating information.

The work was supported at System Associates under Contract Number N60530-79C-0006 using funds supplied to Naval Weapons Center under SSPO Task B0003-SB.

Approved by
E. B. ROYCE, *Head*
Research Department
June 1980

Under authority of
W. B. HAFF
CAPT, U.S. Navy
Commander

Released for publication by
R. M. HILLYER
Technical Director

NWC Technical Publication 6193

Published by Research Department
Collation Cover, 31 leaves
First printing 155 unnumbered copies

UNCLASSIFIED

SECURITY CLASSIFICATION OF THIS PAGE (When Data Entered)

REPORT DOCUMENTATION PAGE		READ INSTRUCTIONS BEFORE COMPLETING FORM
1. REPORT NUMBER NWC TP 6193	2. GOVT ACCESSION NO. AD A097474	3. RECIPIENT'S CATALOG NUMBER
4. TITLE (and Subtitle) DYNAMIC BURNING EFFECTS IN THE COMBUSTION OF SOLID PROPELLANTS WITH CRACKS, AND THE USE OF GRANULAR BED COMBUSTION MODELS		5. TYPE OF REPORT & PERIOD COVERED FINAL 23 OCT 1978 - 30 SEP 1979
		6. PERFORMING ORG. REPORT NUMBER
7. AUTHOR(s) KENNETH K. KUO MRIDUL KUMAR		8. CONTRACT OR GRANT NUMBER(s) N60530-79C-0006
9. PERFORMING ORGANIZATION NAME AND ADDRESS SYSTEMS ASSOCIATES PENNSYLVANIA STATE UNIVERSITY UNIVERSITY PARK, PENNSYLVANIA		10. PROGRAM ELEMENT, PROJECT, TASK AREA & WORK UNIT NUMBERS 64363N B0003-SB
11. CONTROLLING OFFICE NAME AND ADDRESS NAVAL WEAPONS CENTER CHINA LAKE, CALIFORNIA		12. REPORT DATE DECEMBER 1980
		13. NUMBER OF PAGES 58
14. MONITORING AGENCY NAME & ADDRESS (if different from Controlling Office)		15. SECURITY CLASS. (of this report) UNCLASSIFIED
		15a. DECLASSIFICATION/DOWNGRADING SCHEDULE
16. DISTRIBUTION STATEMENT (of this Report) APPROVED FOR PUBLIC RELEASE; DISTRIBUTION UNLIMITED		
17. DISTRIBUTION STATEMENT (of the abstract entered in Block 20, if different from Report)		
18. SUPPLEMENTARY NOTES		
19. KEY WORDS (Continue on reverse side if necessary and identify by block number) SOLID PROPELLANTS COMBUSTION FLAME SPREAD		
20. ABSTRACT (Continue on reverse side if necessary and identify by block number) (SEE BACK OF FORM)		

DD FORM 1473
1 JAN 73EDITION OF 1 NOV 65 IS OBSOLETE
S/N 0102-014-6601

UNCLASSIFIED

SECURITY CLASSIFICATION OF THIS PAGE (When Data Entered)

UNCLASSIFIED

SECURITY CLASSIFICATION OF THIS PAGE(When Data Entered)

(U) *Dynamic Burning Effects in the Combustion of Solid Propellants with Cracks, and the Use of Granular Bed Combustion Models*, by Kenneth K. Kuo and Mridul Kumar. Pennsylvania State University, University Park, Pennsylvania. China Lake, Calif., Naval Weapons Center, December 1980, 58 pp. (NWC TP 6193, publication UNCLASSIFIED.)

(U) This report is a facsimile of a report submitted by Systems Associates, Pennsylvania State University, under Contract N60530-79C-0006 and maintains the original format.

(U) This report summarizes the work performed under the Contract N60530-79C-0006 for the period from October 23, 1978 to September 30, 1979. It includes the study of dynamic burning effects in the combustion of solid propellants with cracks, and the use of granular bed combustion codes for solving hazard problems in rocket propulsion systems.

(U) The Zeldovich quasi-steady flame model was used in the evaluation of the dynamic burning effect. The dynamic burning rate was obtained by solving the transient heat conduction equation for the solid propellant and using the Zeldovich map for determining the heat feedback. Results indicate a stronger dynamic burning response for a higher pressurization rate, larger energy storage in the propellant, and lower initial pressure. A dynamic burning-rate augmentation function was developed to facilitate the incorporation of the transient burning effect into the crack combustion code. The augmentation function is in close correlation with results obtained from the finite difference method over the broad range of conditions studied.

(U) The mobile and fixed granular bed combustion codes (MGBC and FGBC), users manuals for these two programs, sample input data, and output listing were delivered to NWC.

UNCLASSIFIED

SECURITY CLASSIFICATION OF THIS PAGE(When Data Entered)

TABLE OF CONTENTS

	Page
ABSTRACT	1
ACKNOWLEDGMENTS	2
NOMENCLATURE	3
 I. INTRODUCTION	 5
1.1 Dynamic Burning Effects in the Combustion of Solid Propellant Cracks	5
1.1.1 Background	5
1.1.2 Motivation and Objectives	6
1.2 Literature Survey of Recent Studies in Granular Propellant Bed Combustion	7
1.3 Delivery of Fixed and Mobile Granular Bed Combustion Codes (FGBC and MGBC) to NWC and Consultation for the Implementation of the Two Programs	8
 II. DESCRIPTION OF WORK PERFORMED	 9
2.1 Dynamic Burning Effects in the Combustion of Solid Propellant Cracks	9
2.1.1 Theoretical Model	9
2.1.2 Numerical Scheme	15
2.1.3 Implementation of the Dynamic Burning-Rate Program	17
2.1.3.1 Development of Burning-Rate Map for Propellant A	17
2.1.3.2 Dynamic Burning-Rate Subroutine	20
2.1.3.3 Direct Versus Indirect Methods for Incorporating the Dynamic Burning-Rate Subroutine into CCC	23
2.1.4 Calculated Results	24
2.1.5 Development of Burning-Rate Augmentation Function	28
2.1.6 Limitation in the Use of the Dynamic Burning-Rate Augmentation Function	32

TABLE OF CONTENTS, Cont'd.

	Page
2.2 Technological Gaps in the Existing Granular Bed Combustion Models for DDT Studies	43
2.3 Documentation of Fixed and Mobile Granular Bed Combustion Codes (FGBC and MGBC)	46
2.4 Delivery of the Two Programs to NWC and Consultation for their Implementation	47
III. SUMMARY AND CONCLUSIONS	48
IV. REFERENCES	50
APPENDIX I STEADY-STATE BURNING DATA FOR PROPELLANT A	53
APPENDIX II INPUT DATA DESCRIPTION FOR DYNAMIC BURNING RATE PROGRAM	54

Accession For	
NTIS CP&I	<input checked="" type="checkbox"/>
DTIC TAB	<input type="checkbox"/>
Unannounced	<input type="checkbox"/>
Justification	
By	
Distribution/	
Availability Codes	
Dist	Avail and/or Special
A	

ABSTRACT

This report summarizes the work performed under the contract N60530-79-C-0006 for the period from October 23, 1978 to September 30, 1979. It includes the study of dynamic burning effects in the combustion of solid propellants with cracks, and the use of granular bed combustion codes for solving hazard problems in rocket propulsion systems.

The Zeldovich quasi-steady flame model was used in the evaluation of the dynamic burning effect. The dynamic burning rate was obtained by solving the transient heat conduction equation for the solid propellant and using the Zeldovich map for determining the heat feedback. Results indicate a stronger dynamic burning response for a higher pressurization rate, larger energy storage in the propellant, and lower initial pressure. A dynamic burning-rate augmentation function was developed to facilitate the incorporation of the transient burning effect into the crack combustion code. The augmentation function is in close correlation with results obtained from the finite difference method over the broad range of conditions studied.

The mobile and fixed granular bed combustion codes (MGBC and FGBC), users manuals for these two programs, sample input data, and output listing were delivered to NWC.

NWC TP 6193

ACKNOWLEDGMENTS

This research has been sponsored by the Aerothermochemistry Division of the Naval Weapons Center, China Lake, California, under the contract N60530-79-C-0006. The advice and support of Dr. Ronald L. Derr, who served as the technical monitor of this contract, is greatly appreciated. The technical advice of Mr. Channon F. Price, who provided the necessary strand burning data, is also highly appreciated.

The assistance of Mrs. Olivia J. Kuo in implementing the dynamic burning-rate program and conducting parametric studies, and the help of Mr. Vigor Yang in developing the dynamic burning-rate augmentation function for comparison with finite-difference solutions are acknowledged. The authors would like to thank Mr. Gale L. Dargitz for the management of this contract, and Mrs. Patricia Choi for typing the report.

NOMENCLATURE

SYMBOLS

a_1, a_2, a_3, a_4	Dimensionless coefficients used in Eq. (32)
A	Coefficient of the Arrhenius Expression. Eq. (7)
BR	Burning rate augmentation parameter defined in Eq. (30)
b_1, b_2, b_3	Coefficients defined in Eq. (13)
c_1, c_2, c_3	Coefficients defined in Eq. (14)
c	Specific heat at constant pressure
C	Dimensionless parameter used in Eq. (24)
E_a	Activation energy for surface reactions
f	A dimensionless factor used to increase the mesh size in the y direction
k_1, k_2, k_3	Coefficients used in Eq. (33)
P	Pressure
P_i	Initial pressure
PI	Dimensionless initial pressure defined in Eq. (31)
PR	Dimensionless pressurization rate defined in Eq. (28)
r_b	Burning rate of the propellant
R_u	Universal gas constant
t	Time
T	Temperature
y	Vertical distance measured from the propellant surface

NOMENCLATURE Cont'd.

SYMBOLS

α	Thermal diffusivity
λ	Thermal Conductivity
ρ	Density
σ_p	Propellant temperature sensitivity
τ	Dimensionless time defined in Eq. (29)
τ_g	Characteristic time of the gaseous flame
τ_p	Transient pressure variation time (characteristic time of the pressure variation)
τ_s	Characteristic time of the unburned solid phase
ϕ_s	The temperature gradient at the propellant surface

SUBSCRIPTS

g	Gas
i	i^{th} nodal point as shown in Fig. 1, or initial condition
pr	Propellant
ps	Propellant surface

SUPERSCRIPTS

j	j^{th} time step
*	reference quantities
o	steady-state conditions

I. INTRODUCTION

1.1 Dynamic Burning Effects in the Combustion of Solid Propellant Cracks

1.1.1 Background

In solid rocket propulsion systems, the instantaneous burning rate of a solid propellant under rapidly changing non-steady pressure conditions differs greatly from the steady-state burning rate value corresponding to the same pressure. In general, dynamic burning is most frequently encountered under highly transient conditions, especially during the ignition and extinction phases of combustion processes. The deviant burning behavior that occurs during these periods alters the combustion chamber dynamics and flame-spreading rates, thus directly influencing system performance. For example, both the thrust level and the burning time of a high-performance solid rocket may be significantly altered because they depend upon the burning rate of the propellant.

The dynamic burning behavior of solid propellants has been investigated by various researchers, both theoretically and experimentally. An extensive literature review of the research work on dynamic burning is given in Ref. 1.

Physically, the dynamic burning effect is introduced during rapid pressure changes caused by the finite time interval required for the temperature profile of the condensed phase to follow transient pressure variations (Ref. 2). Under an extremely rapid pressure excursion, the temperature profiles in the gaseous-flame and surface-reaction zones may also lag behind the pressure variation. The deviation of the transient burning rate from the steady-state burning rate depends upon two opposing phenomena: (a) the preheating effect of the propellant surface, and (b) the out-of-phase blowing effect of the chemically reacting gases adjacent

to the burning surface. The net result of these phenomena may result in a burning-rate overshoot. Experiments indicate that, in addition to these two primary effects, there are often numerous secondary effects which may influence the heat feedback to the propellant surface and therefore alter the instantaneous burning rate. Secondary effects may include change of chemical kinetics in the flame zone, change of flame luminosity, change of the fraction of instantaneous heat fluxes to fuel binder and oxidizer surfaces, etc. These interrelated physical phenomena are illustrated in the flow chart given in Ref. 1.

The conditions under which the effect of dynamic burning is important are: (1) if the characteristic times associated with the gaseous flame, τ_g , and the solid propellant, τ_s , are not negligibly small in comparison with that of the transient pressure variation time, τ_p ; or (2) if the thermal wave penetration depth is large enough for the initial preheating effects to introduce a significant burning-rate augmentation effect. In the convective burning of a solid propellant with initially open or submerged cracks, the pressure variation time can be extremely short, especially during the transition from convection burning to detonation. Therefore, the dynamic burning effect could be important in the flame-spreading and crack-combustion processes.

1.1.2 Motivation and Objectives

In the theoretical model developed at The Pennsylvania State University³⁻⁵ to describe the combustion processes in solid-propellant cracks, the effect of dynamic burning has not yet been taken into account. However, under certain conditions the dynamic burning effects cannot be ignored. More specifically, the dynamic burning behavior becomes important when the characteristic time associated with the unburnt condensed phase is of the same order of magnitude or greater than that associated with the transient pressure variation. The investigation of the dynamic burning behavior in a solid propellant crack is, therefore, of considerable importance.

The objective of the dynamic burning study are as follows:

1. To improve the crack combustion code to account for the dynamic burning by incorporating a suitable dynamic burning model.
2. To evaluate the significance of dynamic burning by conducting a parametric study for different pressurization rates, initial pressure, and initial subsurface temperature profiles.
3. To develop a burning-rate augmentation function for efficient computation, and to include it into the crack combustion program.

1.2 Literature Survey of Recent Studies in Granular Propellant Bed Combustion

Combustion of granular propellants under a strong confinement may lead to the transition from deflagration to detonation. A number of models have been proposed to simulate the processes of granular propellant combustion. These models were developed for the study of gun interior ballistics. A comparison of the theoretical models, and experimental measurement techniques is summarized in Ref. 6.

It is the purpose of the literature survey to summarize additional research investigations made in this area, following the 1975 JANNAF workshop.⁶ The literature survey is aimed particularly at the applicability of existing theoretical models for the simulation of rocket propulsion problems associated with the deflagration-to-detonation transition (DDT). The survey will also aid in determining the technological gaps and inadequacies of existing models used in DDT studies.

1.3 Delivery of Fixed and Mobile Granular Bed Combustion Codes (FGBC and MGBC) to NWC and Consultation for the Implementation of the Two Programs

In recent years the Principal Investigator has developed two granular bed combustion (GBC) models. One was designed for a fixed bed and the other for a mobile bed. The mobile granular bed combustion (MGBC) model is more general than the fixed granular bed combustion (FGBC) model since the motion of the propellant grain is considered in MGBC. However, the computation time for the mobile bed is considerably longer in comparison to that of the fixed bed. Depending upon the nature of the problem, one model may have advantages over the other. These programs have been successfully executed on the IBM 370 computer, but may require modifications for other types of computers. The users at NWC may also need a certain amount of help and consultation in implementing these programs. Since written documentation of these programs was not available, manuals for users of the programs should be prepared.

II. DESCRIPTION OF WORK PERFORMED

2.1 Dynamic Burning Effects in Combustion of Solid Propellant Cracks

2.1.1 Theoretical Model

As pointed out in the Introduction, the dynamic burning model takes into consideration the time lag for the variation of the temperature profile in the solid propellant under a pressure excursion. This time lag manifests itself in a time-dependent burning, called the dynamic burning. In general, the dynamic burning rate is a function of the pressurization rate, local pressure, and the physiochemical properties of the propellant. The following assumptions have been made in the analysis for mathematical tractability of the problem:

1. The gas-phase reaction zone is considered to be quasi-steady. In other words, because the relaxation time associated with the flame is much shorter than that associated with transient pressure variation, the flame adjusts itself immediately to chamber conditions.
2. No subsurface chemical reactions are present. All chemical reactions are confined to the propellant surface or in the gas phase.
3. Propellant surface temperature is uniform and the propellant is homogeneous.
4. Cross-flow velocities at the propellant surface are small; therefore, no simultaneous erosive-burning effect is present.

The validity of assumption 1 can be shown by comparing the characteristic times associated with the pressure variation, the condensed phase, and the gaseous flame zone. In the crack combustion experiments, the typical time associated with the pressure excursion is in the order of 1 ms. The two other characteristic times are evaluated as follows:

$$\tau_s = \alpha_{pr} / r_b^2 \approx 1.8 \text{ ms} \quad \text{for } r_b = 1 \text{ cm/s} \quad (1)$$

$$\tau_g = \frac{\lambda_g \rho_g c_{pr}}{\lambda_{pr} \rho_{pr} c_g} \tau_s \approx 0.01 \tau_s = 0.018 \text{ ms} \quad (2)$$

Since $\tau_g \ll \tau_p$, the quasi-steady flame assumption is valid. It is also clear that τ_s and τ_p are of the same order of magnitude; therefore, the dynamic burning effect must be considered.

Assumption 2 is reasonable for AP-based composite solid propellants in the pressure range of interest. Even though some propellants may have subsurface heat release, the heat release zone is so thin and so close to the surface that any subsurface heat release can be lumped with surface heat release.

Assumption 3 is employed for mathematical simplicity. It allows the use of a one-dimensional transient heat conduction equation for the solid. Researchers in the field have not as yet investigated the three-dimensional treatment of heat conduction processes in composite solid propellants because of the complexities associated with the three-dimensional structure of oxidizer crystals and fuel binder and the fact that numerical solutions are cumbersome and time consuming.

Assumption 4, that there is no erosive burning effect, is not valid near the crack opening region. However, this assumption does not necessarily introduce significant error in the overall prediction of the combustion processes in cracks, especially for long cracks with high degree of tortuosity.

Methods generally used for solving the quasi-steady flame model can be classified into the following categories:

1. dP/dt method
2. Flame description method
3. Zeldovich method

The dP/dt approach is restricted to those cases which deviate only slightly from the steady state, and thus is not suitable for the crack combustion problem. The flame description approach is inconvenient since it often requires detailed knowledge of the flame structure and propellant surface reaction phenomena.¹

The Zeldovich approach appears to be most suitable for the study of dynamic burning in solid propellant cracks. In this model, the uncertainties of modelling a solid propellant flame are bypassed, and the measurable steady-state burning characteristics are used to deduce the non-steady heat feedback. This method can be used as long as the quasi-steady flame assumption is valid.²

The governing equation for the solid propellant is provided by the following one-dimensional transient heat conduction equation:

$$\frac{\partial T_{pr}}{\partial t} = r_b \frac{\partial T_{pr}}{\partial y} + \alpha_{pr} \frac{\partial^2 T_{pr}}{\partial y^2} \quad (3)$$

where y is measured from the instantaneous propellant crack surface at any axial location as shown in Fig. 1.

The initial and boundary conditions are:

$$T_{pr}(0, y) = T_{pi}, \quad (4)$$

$$T_{pr}(t, \infty) = T_{pi}, \quad (5)$$

$$\frac{\partial T_{pr}}{\partial y}(t, 0^+) = \dot{\phi}_s(t). \quad (6)$$

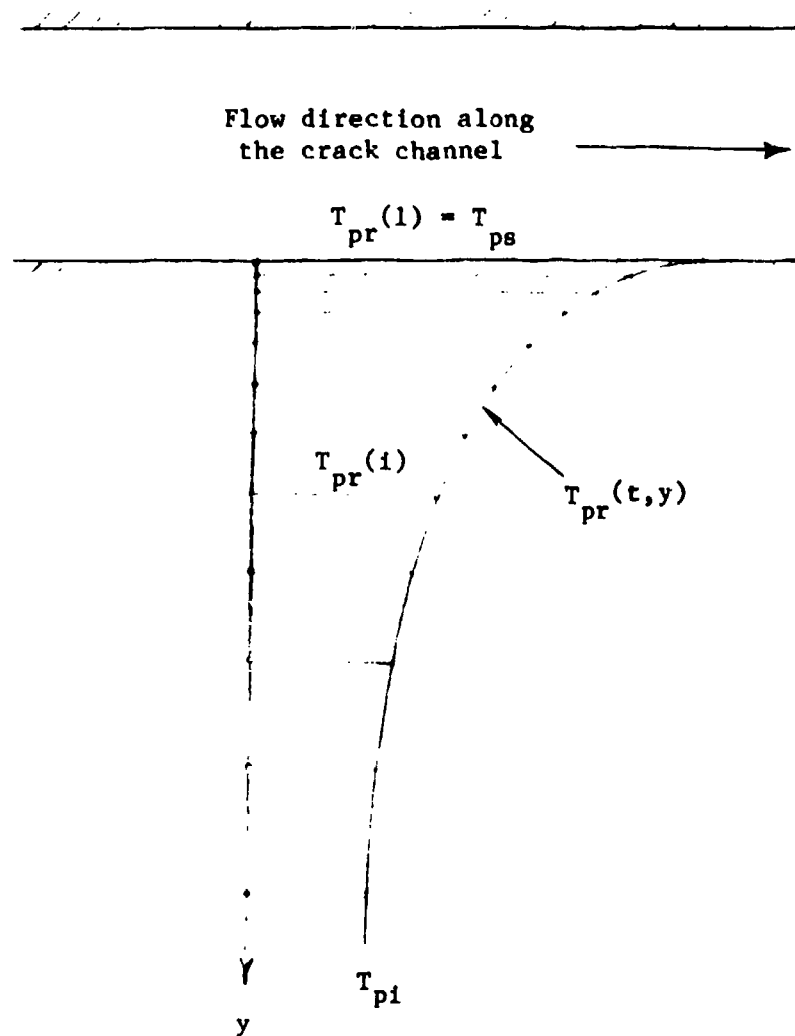


FIG. 1 Description of the physical model.

Before ignition of the propellant at a given axial location, the burning rate r_b , in Eq. (3) is zero and the subsurface temperature gradient ϕ_s is obtained from a well-established empirical correlation (Dittus-Boelter's correlation) for convective heat transfer in a flow channel.

After the onset of ignition, the instantaneous burning rate is related to the propellant surface temperature by an Arrhenius pyrolysis expression:

$$r_b(t) = A e^{-\frac{E_a}{R_u T_{ps}}} \quad (7)$$

The subsurface temperature gradient in a functional form can be written as

$$\phi_s(t) = \phi_s[r_b(t), p(t)] \quad (8)$$

Following Zeldovich's concept of quasi-steady flame, this function is the same as that obtained from steady-state burning conditions. A schematic drawing showing the method for obtaining the burning rate map [$\phi_s = \phi_s(r_b, P)$] from the steady-state experimental data is shown in Fig. 2. Essentially, the dynamic burning-rate map is constructed through the use of (a) the pyrolysis data, (b) the measured steady-state burning rate as a function of pressure and initial temperature, and (c) the following algebraic relationship,

$$\phi_s = \frac{r_b}{\alpha_{pr}} (T_{ps} - T_{pi}) \quad (9)$$

which represents the surface heat flux for steady-state burning. Detailed justification for this procedure can be found in Ref. 2.

STEADY-STATE EXPERIMENTAL DATA

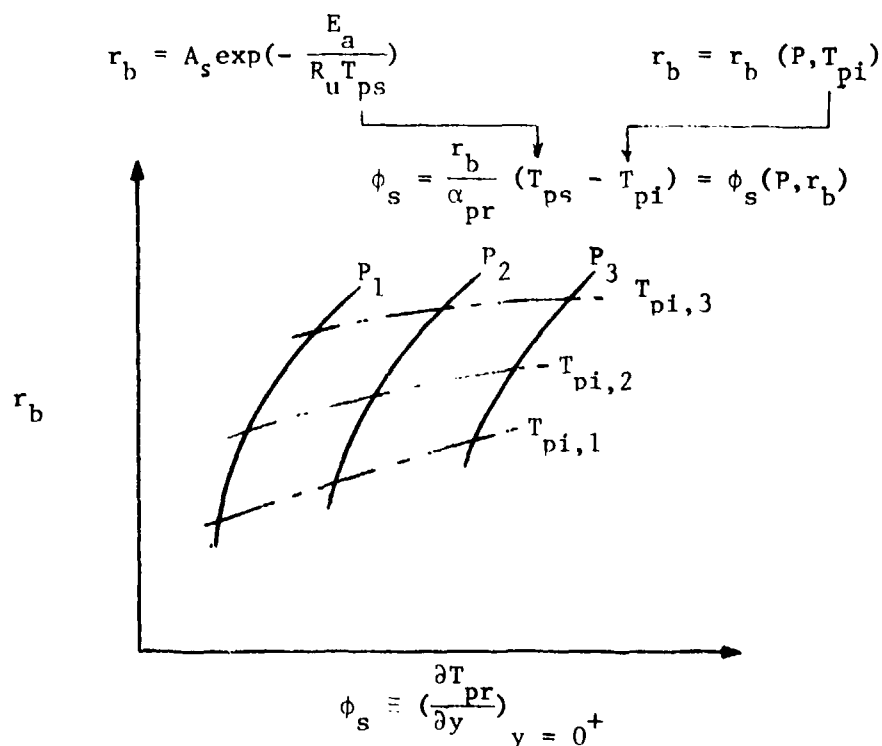
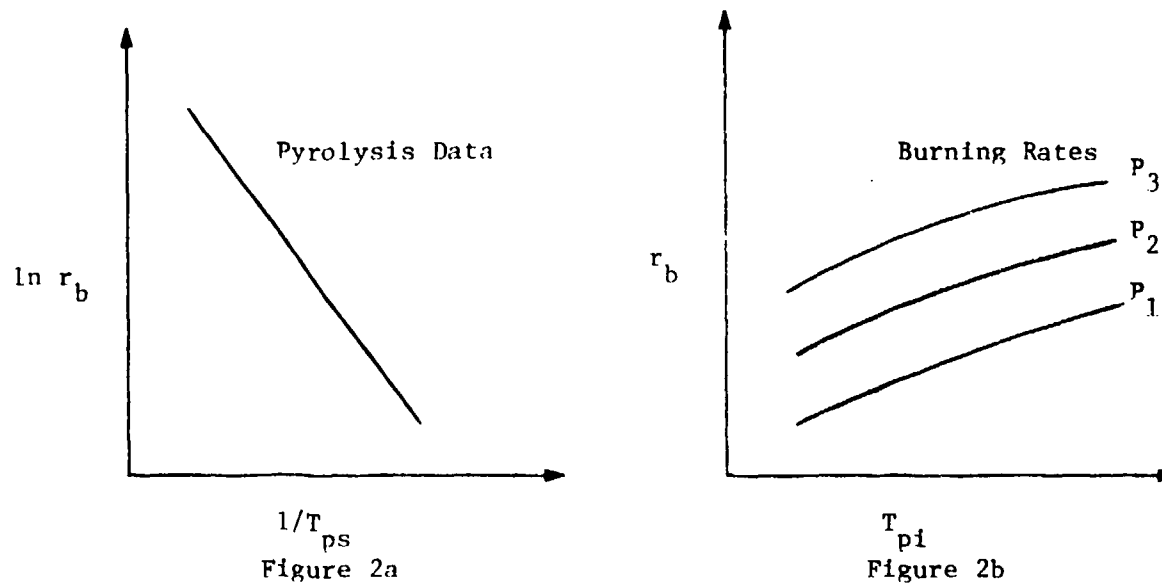


Figure 2c

Fig. 2 Schematic drawing showing the procedure to obtain the heat feedback function from steady-state data

2.1.2 Numerical Scheme

The governing partial differential equation for the solid phase, Eq. (3), was solved by using an implicit finite difference technique with a variable mesh system. The variable grid spacing provides finer grid spacing near the surface. The central-difference method was used to approximate both time and spatial derivatives. When T_i^j represents $T(j\Delta t, y_i)$, the finite difference approximation for the time and spatial derivatives are:

$$\left. \frac{\partial T}{\partial t} \right|_i^{j+\frac{1}{2}} = \frac{T_i^{j+1} - T_i^j}{\Delta t} \quad (10)$$

$$\left. \frac{\partial T}{\partial y} \right|_i^j = \frac{b_1 T_{i-1}^j + b_2 T_i^j + b_3 T_{i+1}^j}{y_i - y_{i-1}} \quad (11)$$

$$\left. \frac{\partial^2 T}{\partial y^2} \right|_i^j = c_1 \left[\frac{T_{i-1}^j - c_2 T_i^j + c_3 T_{i+1}^j}{(y_i - y_{i-1})^2} \right] \quad (12)$$

where

$$b_1 = -\frac{1+f}{2+f}, \quad b_2 = \frac{f}{1+f}, \quad b_3 = \frac{1}{(1+f)(2+f)} \quad (13)$$

$$c_1 = \frac{2}{2+f}, \quad c_2 = \frac{2+f}{1+f}, \quad c_3 = \frac{1}{1+f} \quad (14)$$

The factor, f , is used to increase the mesh size in the y direction:

$$y_{i+1} - y_i = \Delta y_i = (1+f) \Delta y_{i-1} \quad (15)$$

Using the above finite difference approximations, the transient heat conduction equation can be expressed in the following form:

$$\begin{aligned} \frac{T_i^{j+1} - T_i^j}{\Delta t} = & \frac{r_b^{j+\frac{1}{2}}}{2 \Delta y_{i-1}} [b_1 (T_{i-1}^{j+1} - T_{i-1}^j) + b_2 (T_i^{j+1} + T_i^j) + b_3 (T_{i+1}^{j+1} + T_{i+1}^j)] \\ & + \frac{a_{pr} c_1}{2 (\Delta y_{i-1})^2} [(T_{i-1}^{j+1} + T_{i-1}^j) - c_2 (T_i^{j+1} + T_i^j) + c_3 (T_{i+1}^{j+1} + T_{i+1}^j)] \end{aligned} \quad (16)$$

It should be noted that the subscript pr for temperature has been dropped here for brevity. Eq. (16) was linearized by approximating the burning rate at the intermediate time step, with the average value calculated between the previous time value and the current time value in the last iteration, i.e.,

$$r_{b_i}^{j+1} = \frac{1}{2} (r_{b_i}^j + r_{b_i}^{j+1,k}) \quad (17)$$

for the $(k+1)$ th iteration.

The following expression is used at the solid boundary:

$$\left. \frac{\partial T}{\partial y} \right|_1^{j+1} = \phi_s \quad (18)$$

where ϕ_s is obtained through the burning-rate map, details of which are given in the next section. The left-hand side of Eq. (18) is approximated by a three-point backward difference method, and is represented by

$$\left. \frac{\partial T}{\partial y} \right|_1^{j+1} = \frac{-\beta^2 (T_3^{j+1} - T_1^{j+1}) + (1+\beta)^2 (T_2^{j+1} - T_1^{j+1})}{(1+\beta) y_1} \quad (19)$$

where $\beta \equiv 1/(1+f)$.

For the last nodal point ($i = i_{\max}$),

$$T_{i_{\max}} = T_{pi} \quad (20)$$

The resulting set of simultaneous algebraic equations was solved by using a standard tridiagonal matrix inversion. The propellant surface temperature thus obtained was used in the Arrhenius expression, Eq. (7), to obtain the new burning rate. This burning rate was then used to obtain ϕ_s from the burning-rate map. The temperature profile was recomputed, based upon the new value of ϕ_s ; before advancing to the next time step, the cycle was continued until the solution converged.

2.1.3 Implementation of the Dynamic Burning-Rate Program

2.1.3.1 Development of Burning-Rate Map for Propellant A

The Zeldovich burning-rate map was constructed, using the steady-state burning rate data supplied by Mr. C. F. Price of NWC (see Appendix I). To increase the number of data points at different pressures and initial temperatures, additional intermediate data were generated through interpolation to facilitate map reading. Fig. 3 gives the burning rate versus initial propellant temperature for different pressures. An average temperature sensitivity coefficient of the burning rate was also obtained from the data. The temperature sensitivity is needed to extrapolate the available experimental data for obtaining the propellant initial temperature below the range of data supplied by NWC. The average value of the temperature sensitivity coefficient was found to be

$$\sigma_p \equiv \left(\frac{\partial \ln r_b}{\partial T_{pi}} \right)_p = 0.00132 \text{ K}^{-1} \quad (21)$$

The burning rate was plotted against $1/T_{ps}$ for various pressures. As seen in Fig. 4, one line fits all the data well, regardless of the pressure. The functional expression for this line was obtained in the Arrhenius form given by

$$r_b = A_s \exp \left(- \frac{E_a}{R_u T_{ps}} \right) \quad (22)$$

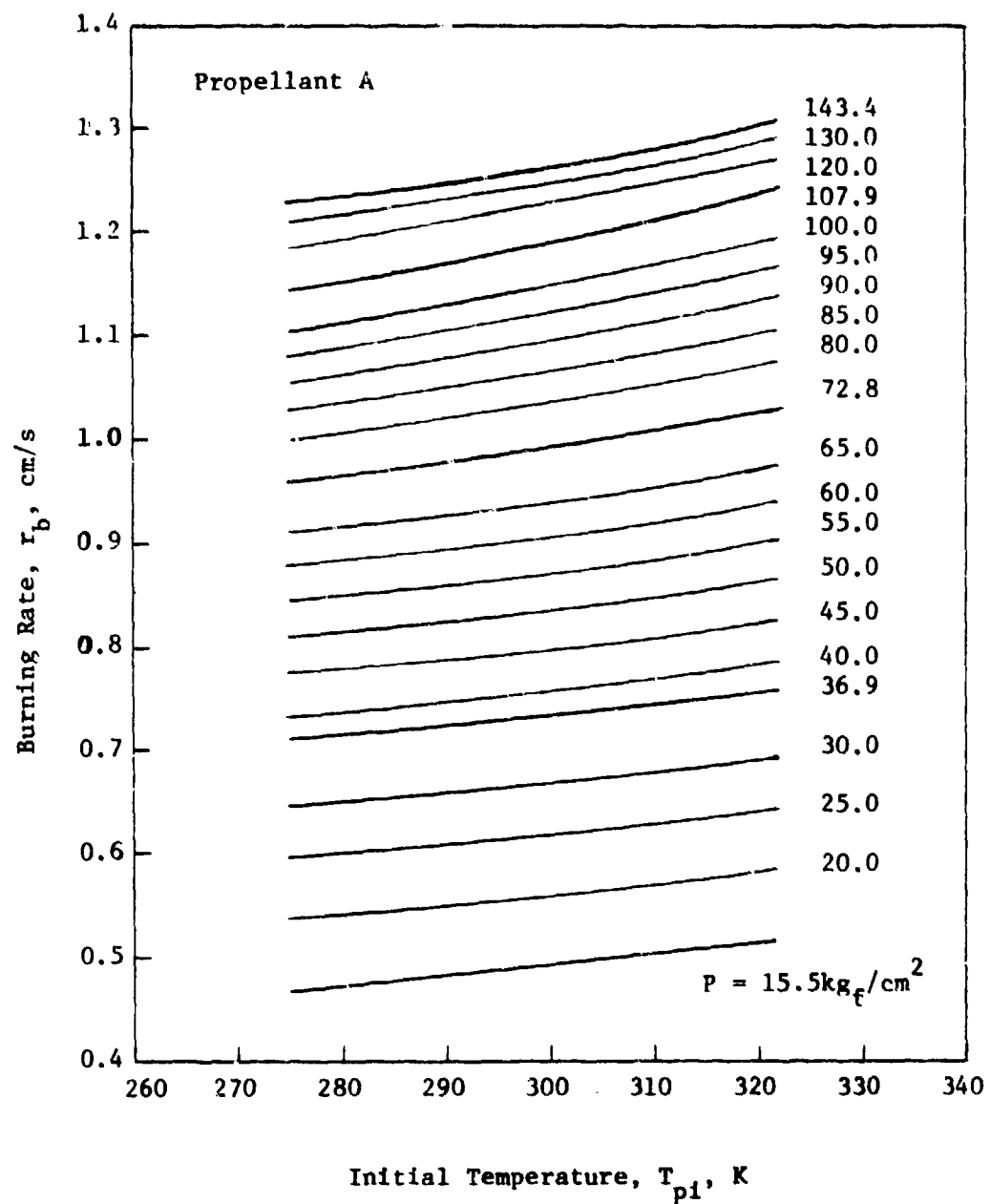


Fig. 3 Steady-state burning rate for various initial propellant temperatures and pressures

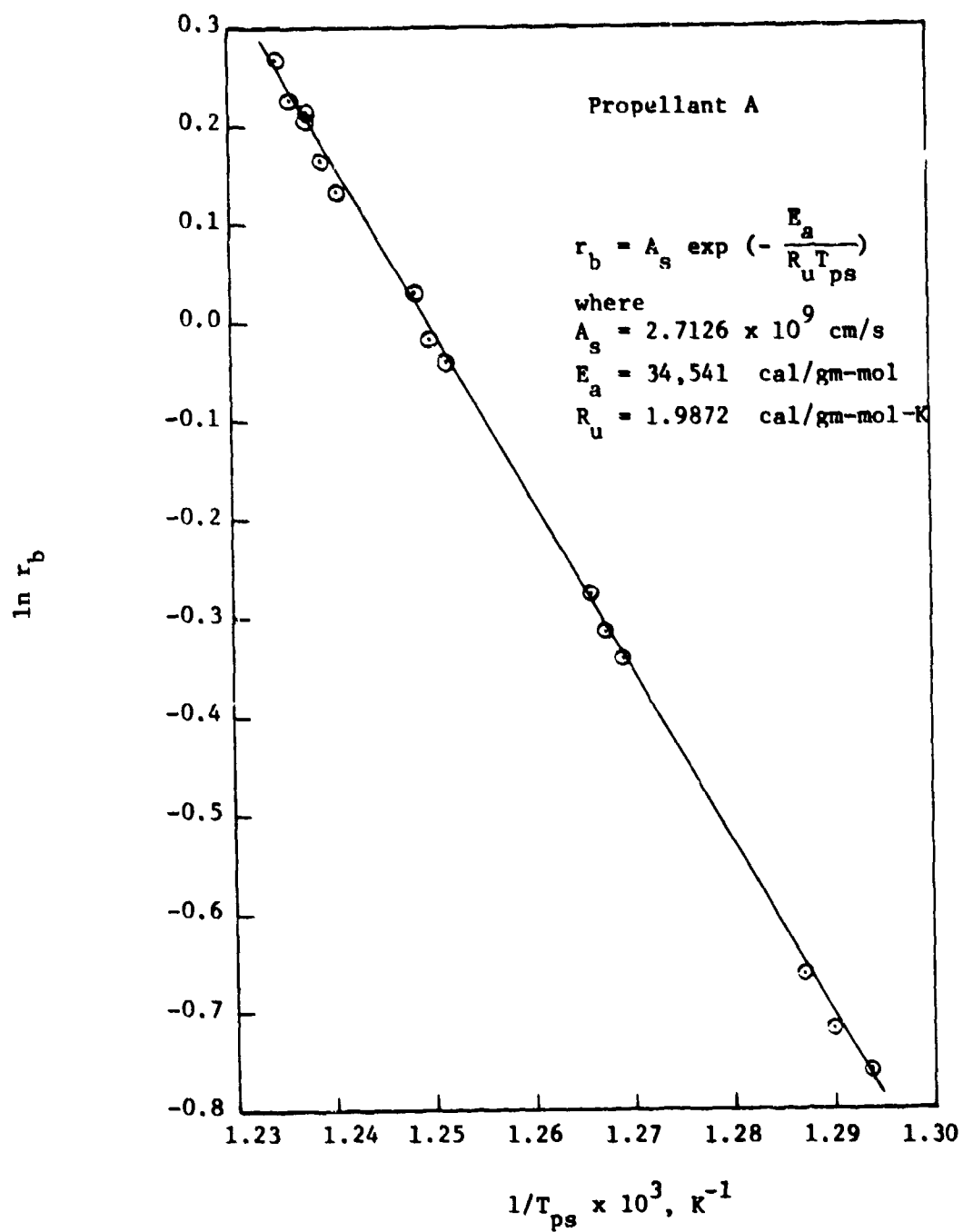


Fig. 4 Burning rate vs propellant surface temperature

where $A_g = 2.7126 \times 10^9$ cm/sec

$E_a = 34,541$ cal/gm-mole

$R_u = 1.9872$ cal/gm-mole $^{\circ}$ K

According to the procedure outlined in Fig. 2, a plot of $\phi_g(P, r_b)$ was obtained, as shown in Fig. 5. Unfortunately, it is nearly impossible to interpolate ϕ_g for different values of r_b and P because of the steepness of the isobaric lines and the scarcity of the data points. Accordingly, this plot is not used, instead, Fig. 3 and Eq. (22) are used together with Eq. (9) to obtain ϕ_g . An interpolation routine, based upon the Aitken-Lagrange interpolation method, was implemented to interpolate data (plotted on Fig. 3) for obtaining an equivalent initial propellant temperature $T_{pi_{eq}}$. Detailed procedures for computing the dynamic burning rate are given in the next section.

2.1.3.2 Dynamic Burning-Rate Subroutine.

After the onset of ignition, the burning-rate subroutine is used to compute the instantaneous burning rate. First, the values of the burning rate and propellant surface temperature are assumed. The burning-rate map, Fig. 3, is interpolated to obtain the equivalent initial propellant temperature. The heat feedback, ϕ_g , is calculated from Eq. (9). The transient heat conduction equation is solved by using a new value of ϕ_g to obtain a new propellant temperature profile and surface temperature, T_{ps} . A new burning rate is determined from the Arrhenius expression, Eq. (22). The burning-rate map is used again to obtain new equivalent initial propellant temperature. This procedure is repeated until the solution converges. The converged burning rate is the desired dynamic burning rate. A general layout of the dynamic burning-rate subroutine is given in Fig. 6.

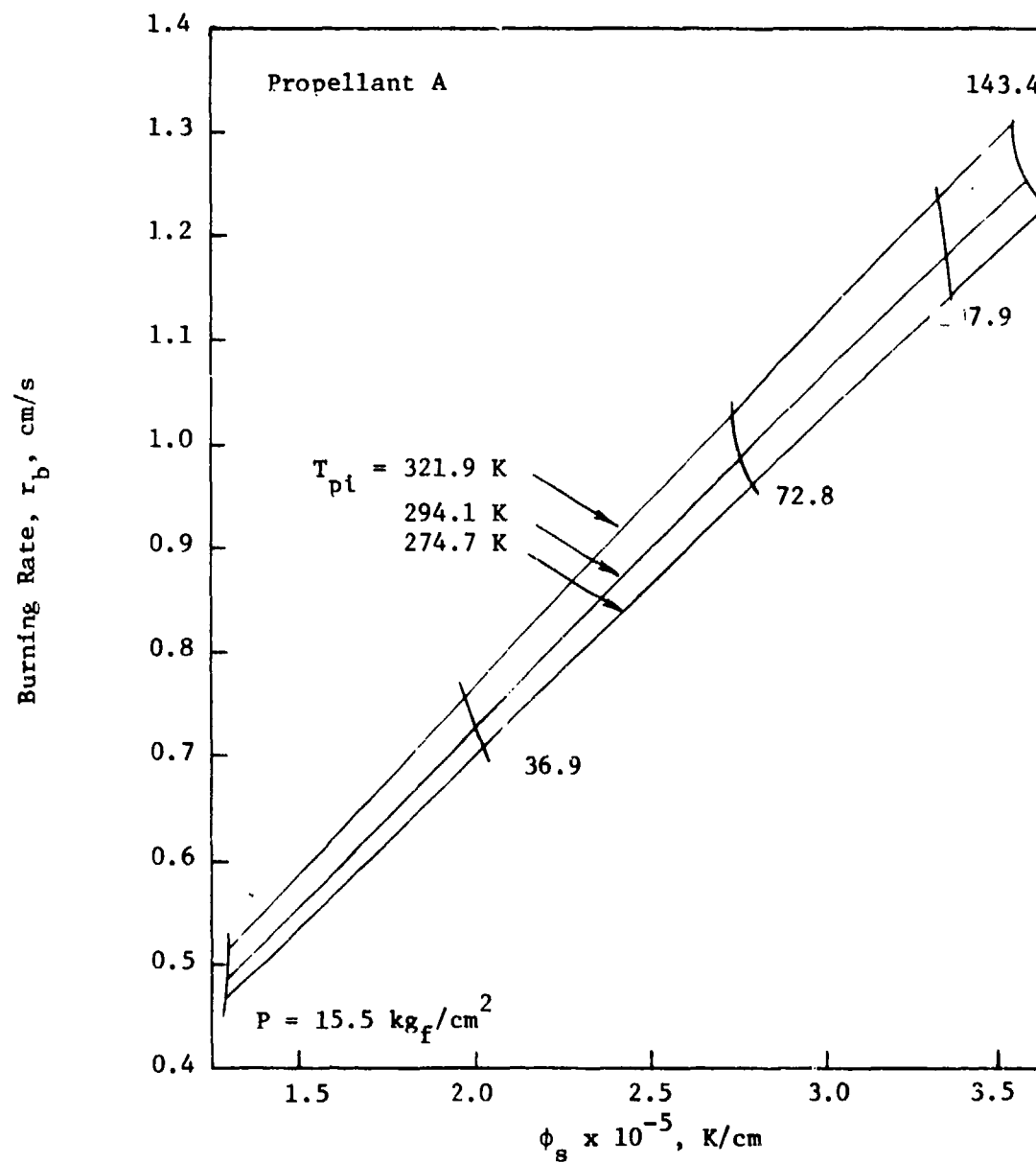


Fig. 5 Zeldovich map constructed from steady-state burning rate data

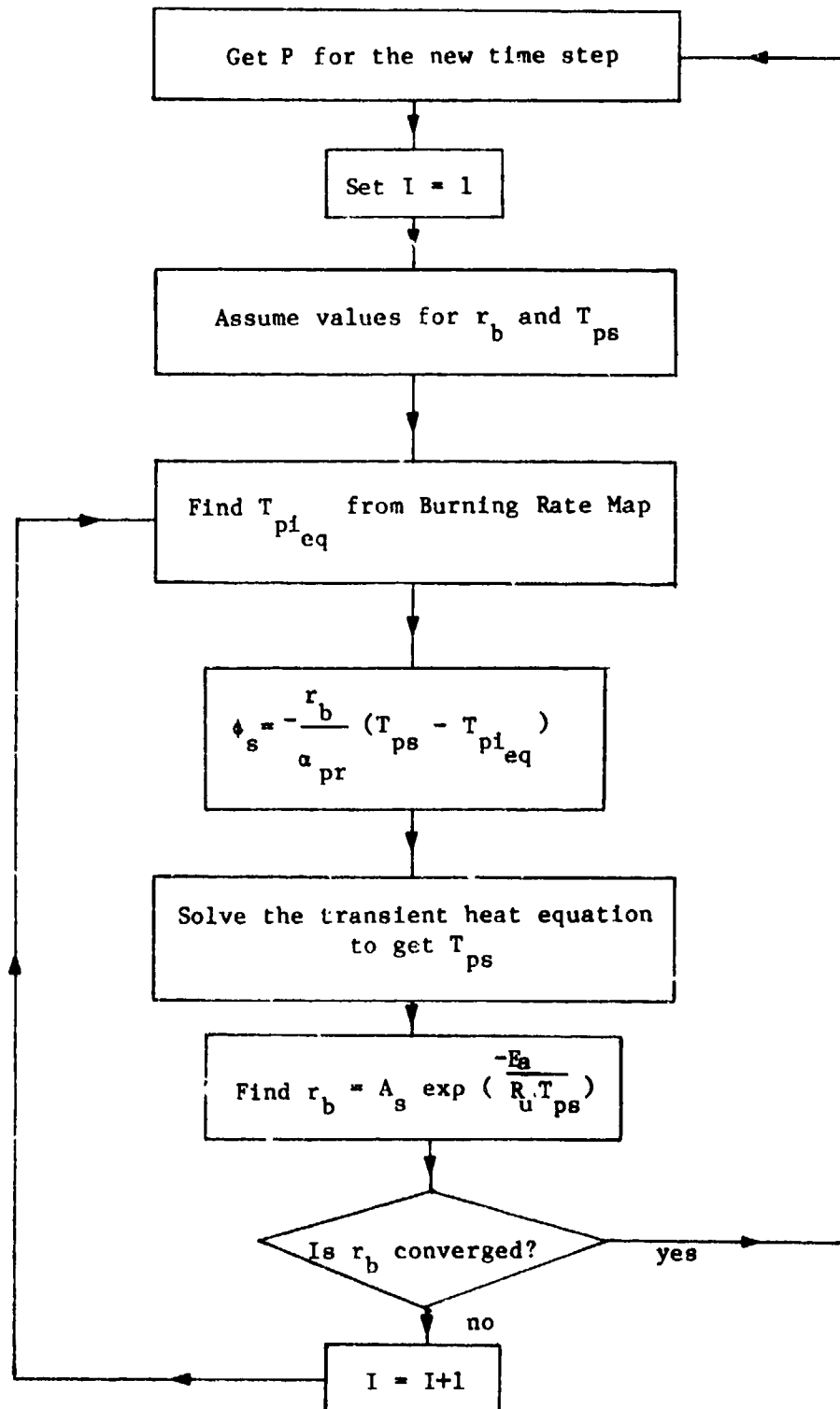


FIG. 6 Flow Chart of the Computation Procedure used in Dynamic Burning Rate Program

During the calculation, if the burning rate goes below the value corresponding to that at 274.7 K, the equivalent initial temperature is obtained by using the temperature sensitivity coefficient

$$\sigma_p \cdot (T_{f_{1eq}}) = 274.7 - \frac{1}{\sigma_p} \ln \left\{ \frac{[r_b(P)]_{274.7 \text{ K}}}{[r_b(P)]} \right\} \quad (23)$$

2.1.3.3 Direct Versus Indirect Methods for Incorporating the Dynamic Burning-Rate Subroutine into CCC

The dynamic burning-rate routine and the burning-rate map were coupled directly into the crack combustion code (CCC). Several runs were made with this coupled program. The following general observations about the coupled program were made:

1. Depending upon the temperature profile at the onset of gasification, extinction may immediately follow, due to the shallow subsurface temperature profile.
2. $\partial P / \partial t$ has a very strong influence on burning-rate augmentation.
3. In order to obtain a convergent solution, the time increment for the coupled program must be an order of magnitude smaller than that for CCC alone. This results in a substantial increase of the computer time for each run.

In view of the substantial increase in computation time, it was concluded to be more pragmatic and economical to develop a burning-rate augmentation function. Results obtained from a systematic variation of parameters (such as $\partial P / \partial t$, propellant subsurface temperature profile, etc.) can be used to obtain such a function.

In the development of burning-rate augmentation function, the effect of subsurface temperature profile at the onset of ignition has to be considered. A reasonable representation of the temperature profile would be an exponential form. Therefore, the following exponential distribution of the subsurface temperature profile was used:

$$\frac{T_{pr} - T_{pi}}{T_{ps} - T_{pi}} = e^{-\frac{r_b y}{a_{pr} C}} \quad (24)$$

It should be noted that when $C = 1$, the temperature profile reduces to that of a steady-state burning. When $C < 1$, the temperature profile will be more shallow than that of the steady-state profile. Therefore, if $C < 1$ at the onset of ignition, no dynamic burning is assumed to take place. In general, at the onset of ignition, the subsurface temperature profile will not be exponential. A least square curve-fit procedure was therefore employed to obtain the equivalent exponential temperature profile at the onset of ignition. In the development of the burning-rate augmentation function, C was used as one of the parameters. The burning-rate augmentation factor is defined as the ratio of the dynamic burning rate at a given pressure to the steady-state burning rate at the same pressure.

2.1.4 Calculated Results

The numerical solution of the dynamic burning effect was studied by two methods: (1) by using a dummy main program with a specified pressurization rate, initial propellant temperature profile, and initial pressures; (2) by directly coupling the dynamic burning-rate subroutine into the crack combustion code. As mentioned in section 2.1.3.3, the time increment for the coupled program must be at least one order of magnitude smaller than that for CCC alone; therefore, for the most part, the first method was used to study the dynamic burning effect.

Fig. 7 is a typical graph showing the effect of pressurization rate on dynamic burning rate augmentation factor, r_b/r_b^0 , for a given pressure and steady-state initial temperature profile. The pressurization rate, $\frac{\partial p}{\partial t}$, was assumed to be constant, with pressure increasing monotonically. The reasons for considering this type of pressurization process are: (1) during the flame-spreading process in a solid propellant crack, the pressurization rate at a given axial location remains more or less constant; (2) a single variable (i.e., the average value of $\frac{\partial p}{\partial t}$) can be used to study the effect of pressurization rate in the parametric study; and (3) during a DDT process, the pressure in the system usually increases monotonically.

A similarity between the shapes of various curves under different pressurization rates can be seen in Fig. 7. The burning-rate augmentation factor starts from 1 at $t = 0$. As time increases, the augmentation factor also increases, reaching a plateau. As time increases further, the curve passes through a point of inflection, and finally reaches a runaway condition. The time required to reach the runaway condition, or the vertical asymptote, decreases as pressurization rate is increased. In other words, the plateau (flat) region of the curve decreases as the pressurization rate is increased, and finally disappears when the pressurization rate is greater than 10^6 atm/s. It is also evident that for pressurization rates above 10^5 atm/s, the dynamic burning rate is important even for short time durations. This implies that the dynamic burning-rate effect may contribute significantly to the DDT process, which usually occurs at very high pressurization rates ($\gg 10^5$ atm/s).

Fig. 8 is similar to Fig. 7, except that the initial temperature profiles at the onset of ablation are different. Figure 8 corresponds to the case, with higher initial thermal energy storage than shown in Fig. 7. By comparing these two figures, the effect of initial temperature profiles can be readily seen. A thicker initial temperature profile (which

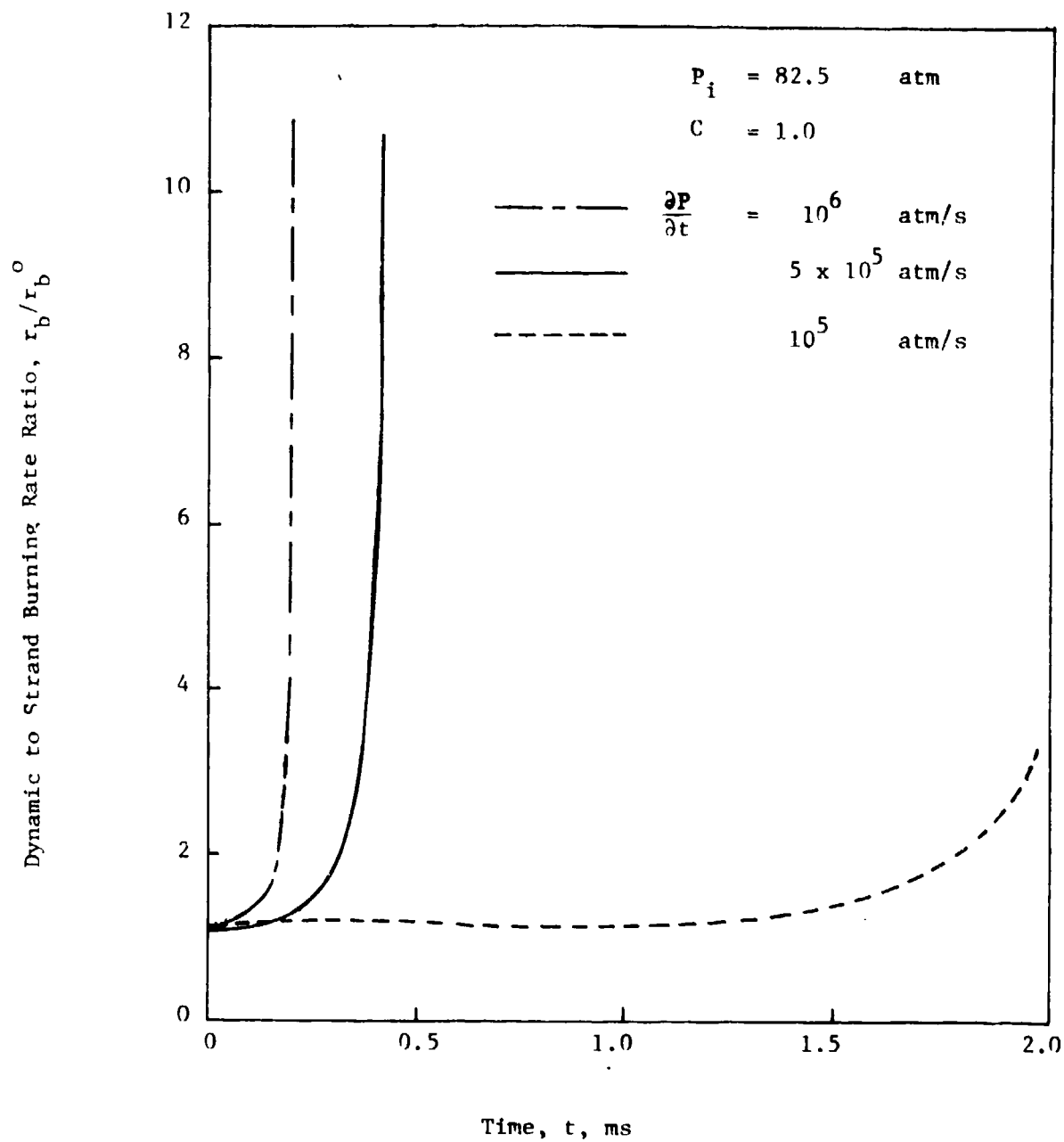


Fig. 7 Calculated dynamic burning rate augmentation factor versus time for $C = 1.0$ and $P_i = 82.5$ atm

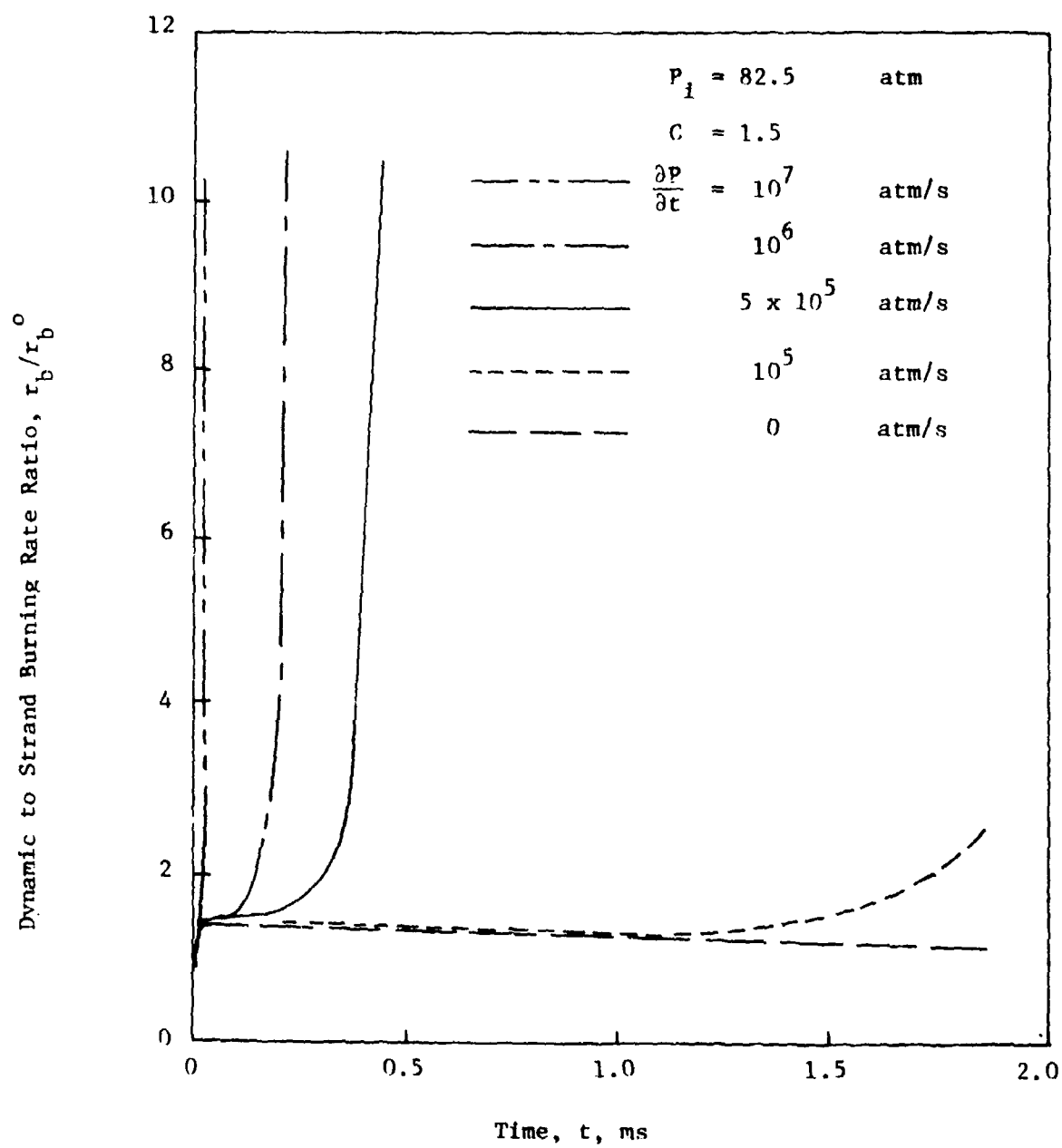


Fig. 8 Calculated dynamic burning rate augmentation factor versus time for $C = 1.5$ and $P_i = 82.5$ atm

corresponds to larger values of parameter C) results in an increased dynamic burning rate. However, the time required to reach the runaway condition remains essentially unaffected by the value of C . Fig. 9 is a plot of burning-rate augmentation factor versus time for $C = 1.5$ and initial pressure of 50 atm. Comparing Figs. 8 and 9, one can see that as the initial pressure is decreased, the general nature of the dynamic burning-rate curves remain constant; however, the curve for a given pressurization rate and initial temperature profile shifts to the left, i.e., the time to reach the runaway condition decreases. This is in agreement with the generally observed pressure effect on dynamic burning.¹

It should be noted that the pressure-time history has a strong influence on the predicted dynamic burning rate. Numerical calculations, with a ramp pressurization followed by a constant pressure period, show that the burning rate declines after reaching a peak, and approaches the steady-state burning rate. These results are also consistent with those reported in previous dynamic burning studies.

The effect of the initial temperature profile, which is thinner than the steady-state profile, has also been studied. It was found that when the initial temperature profile is shallower than the steady-state case, i.e., $C < 1$, the dynamic burning-rate augmentation during a pressurization process is much less pronounced. Under high pressurization rates, the burning rate may first reach a peak followed by a valley and then increase again after a long period of time. At lower pressurization rates, the burning rate may first reach a peak followed by a monotonic decline until extinction is reached. Therefore, the dynamic burning effect is not taken into account for cases with $C < 1$ in the development of the dynamic burning-rate augmentation function.

2.1.5 Development of Burning-Rate Augmentation Function

Several sets of data were generated by using the dynamic burning-rate subroutine to facilitate the development of a burning-rate

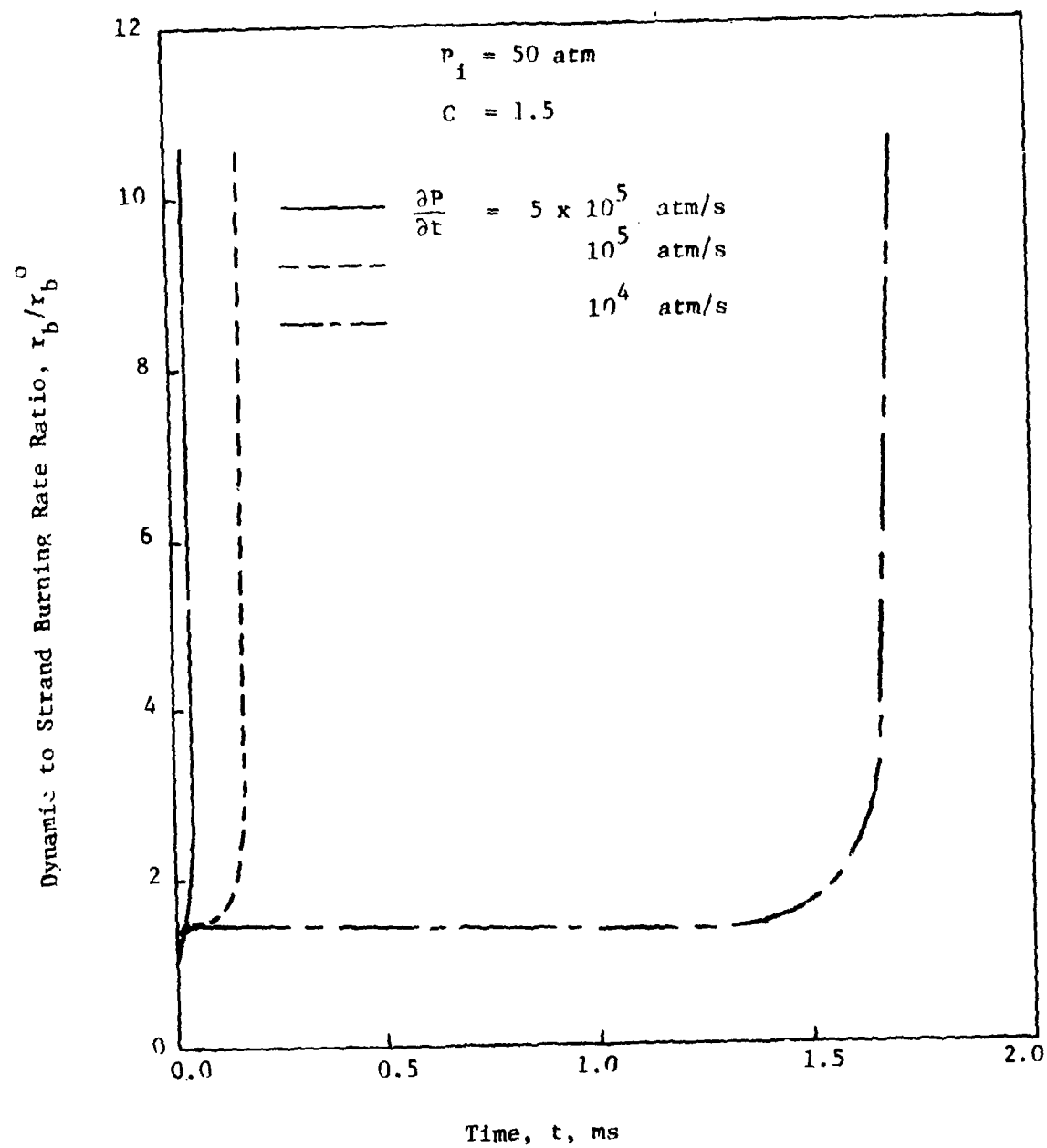


Fig. 9 Calculated dynamic burning rate augmentation factor versus time for $C = 1.5$ and $P_1 = 50$ atm

augmentation function. The parameters used to generate the dynamic burning rate were: the pressurization rate, $\partial P/\partial t$; the initial pressure, P_i ; and the variable C , which governs the shape of the initial temperature profile [see Eq. (24)]. For the sake of generality, the burning-rate augmentation function was developed through the use of a set of dimensionless parameters. The reference parameters used for nondimensionalization are

$$t^* \equiv \frac{a \text{ pr}}{(r_{b_i}^o)^2} \quad (25)$$

$$\left(\frac{\partial P}{\partial t} \right)^* \equiv \frac{P_i}{t^*} \quad (26)$$

where $r_{b_i}^o$ is the steady-state burning rate obtained from Saint-Robert's type of burning rate law:

$$r_{b_i}^o = a P_i^n \quad (27)$$

where $a = 0.9359 \times 10^{-2} \text{ (cm/s)/(g/cm}^2\text{)}^n$
 $n = 0.4108$

The dimensionless parameters are

$$\text{PR} \equiv \left(\frac{\partial P}{\partial t} \right) / \left(\frac{\partial P}{\partial t} \right)^* \quad (28)$$

$$\tau \equiv t/t^* \quad (29)$$

$$\text{BR} \equiv \frac{r_b}{r_{b_i}^o} - 1 \quad (30)$$

$$\text{PI} \equiv \frac{P_i}{P_i^*} \quad \text{where } P_i^* = 50 \text{ atm} \quad (31)$$

Data were generated for eight pressurization rates, $\partial P/\partial t = 0, 10^4, 5 \times 10^4, 10^5, 2 \times 10^5, 5 \times 10^5, 10^6$, and 10^7 atm/s ; three initial propellant

temperature profiles, $C = 1, 1.5$ and 2 ; and three initial pressures, $P_1 = 34, 50$, and 82.5 atm. Since the nature of the curves is very similar, it is possible to obtain a suitable function which can approximate all of the curves. Because the runaway time or the vertical asymptote of the burning rate for a given PR and PI is nearly independent of C , the fast-rising portion of the curves in the later stage can be approximated by

$$BR = a_3 \left[\frac{\tau^{a_2}}{\left(\frac{a_1}{PR} - \tau \right)^{a_4}} \right] \quad (32)$$

where a_1, a_2, a_3 , and a_4 are functions of PI only. In order to obtain a better fit for the entire region, the following functional form was used:

$$BR = \tau^{k_1} (k_2 + k_3 \tau + k_4 \tau^2) + a_3 \left[\frac{\tau^{a_2}}{\left(\frac{a_1}{PR} - \tau \right)^{a_4}} \right] \quad (33)$$

where the functional dependence of k 's are

$$\left. \begin{aligned} k_1 &= k_1(PI, C) \\ k_2 &= k_2(PI, PR) \\ k_3 &= k_3(PI, PR) \\ k_4 &= k_4(PI, PR) \end{aligned} \right\} \quad (34)$$

The coefficients a_1 and a_4 were approximated by second-order polynomials of PI, and are given by

$$\begin{pmatrix} a_1 \\ a_2 \\ a_3 \\ a_4 \end{pmatrix} = \begin{pmatrix} 0.975 & -0.6303 & 1.6235 \\ 0.743 & -0.0384 & 0.1314 \\ 0.465 & -0.1967 & 0.091 \\ 0.5867 & 0.1283 & 0.2781 \end{pmatrix} \begin{pmatrix} 1 \\ PI \\ PI^2 \end{pmatrix} \quad (35)$$

The coefficients k 's are given by

$$k_1 = (0.424 + 0.514 PI + 2.6159 PI^2) - (0.508 + 0.204 PI + 0.1136 PI^2)C + (0.128 - 0.1379 PI + 0.0677 PI^2)C^2 \quad (36)$$

$$k_2 = (1 - PI)(1.673 - 1.81 PR + 0.272 PR^2) \times 10^{16} \quad (37)$$

$$k_3 = (1 - PI)(1.639 - 1.762 PR + 0.2648 PR^2) \times 10^{15} \quad (38)$$

$$k_4 = (1 - PI)(9.226 - 9.98 PR + 1.5 PR^2) \times 10^{17} \quad (39)$$

The coefficients were obtained through the use of an established statistical analysis (SAS) program.⁷ Figures 10 to 18 show the comparison of the dynamic burning rates predicted by the burning-rate augmentation function with those obtained using the dynamic burning-rate program. It can be seen from these plots that the proposed dynamic burning-rate augmentation function represented by Eq. (33) can closely predict the burning rates obtained from the finite difference solution for the range of pressurization rates, initial pressures, and the initial propellant temperature profiles considered in this study. Figures 16 to 18 show the degree of scatter of the burning rates calculated by the two different methods (numerical vs. augmentation function) around the 45° line. It is quite clear that the agreement is good for all three initial pressures considered. Therefore, it is believed that the burning-rate augmentation function can adequately predict the dynamic burning effect.

2.1.6 Limitations in the Use of Dynamic Burning-Rate Augmentation Function

In spite of the close agreement between the burning rates predicted by the augmentation function and those computed by the finite difference method, care should be taken in using the augmentation function beyond the range of parameters studied. It should also be noted that the application of the augmentation function is limited because of the following constraints:

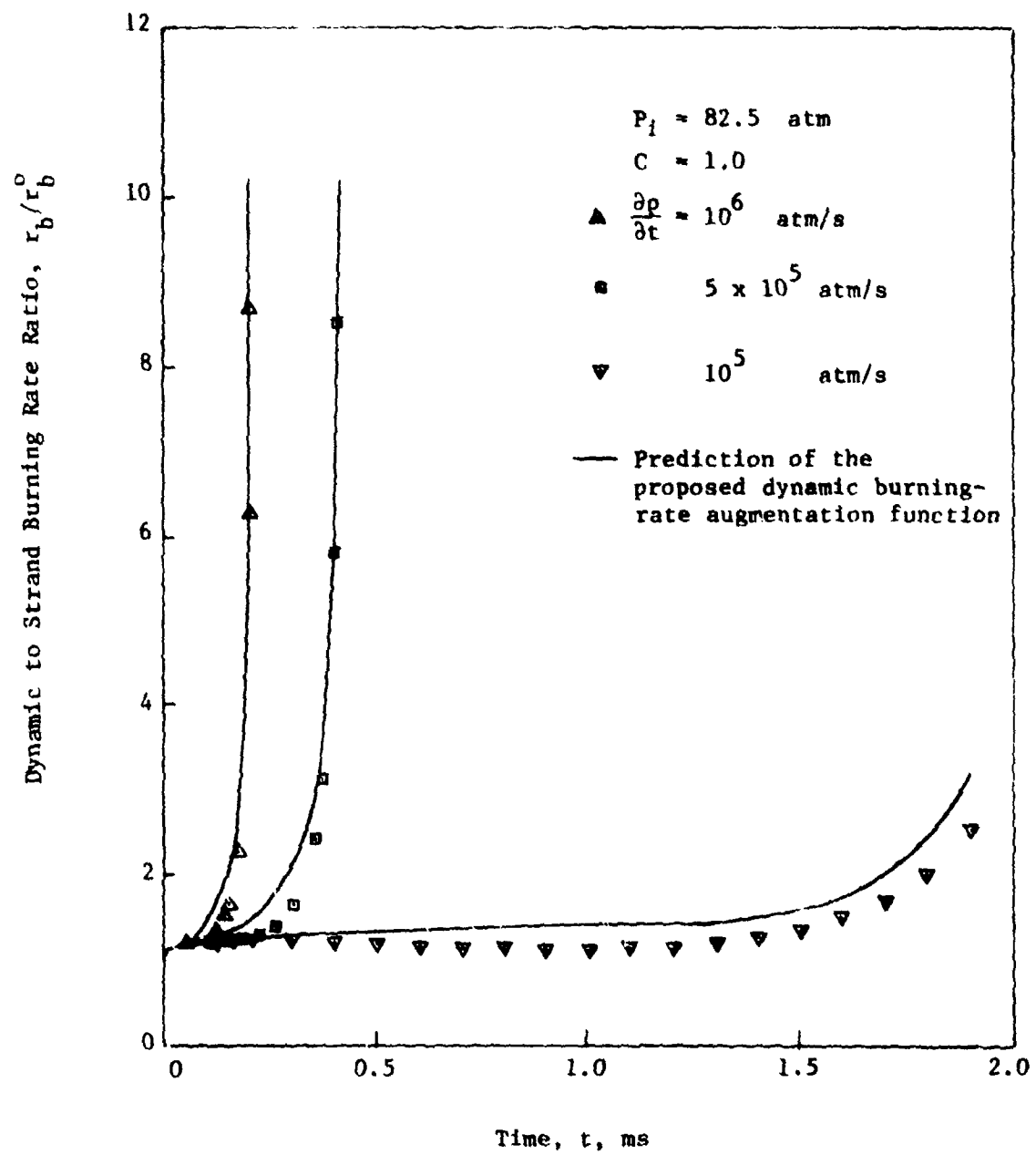


Fig. 10 Comparison of the dynamic burning rate data with the prediction from burning rate augmentation function

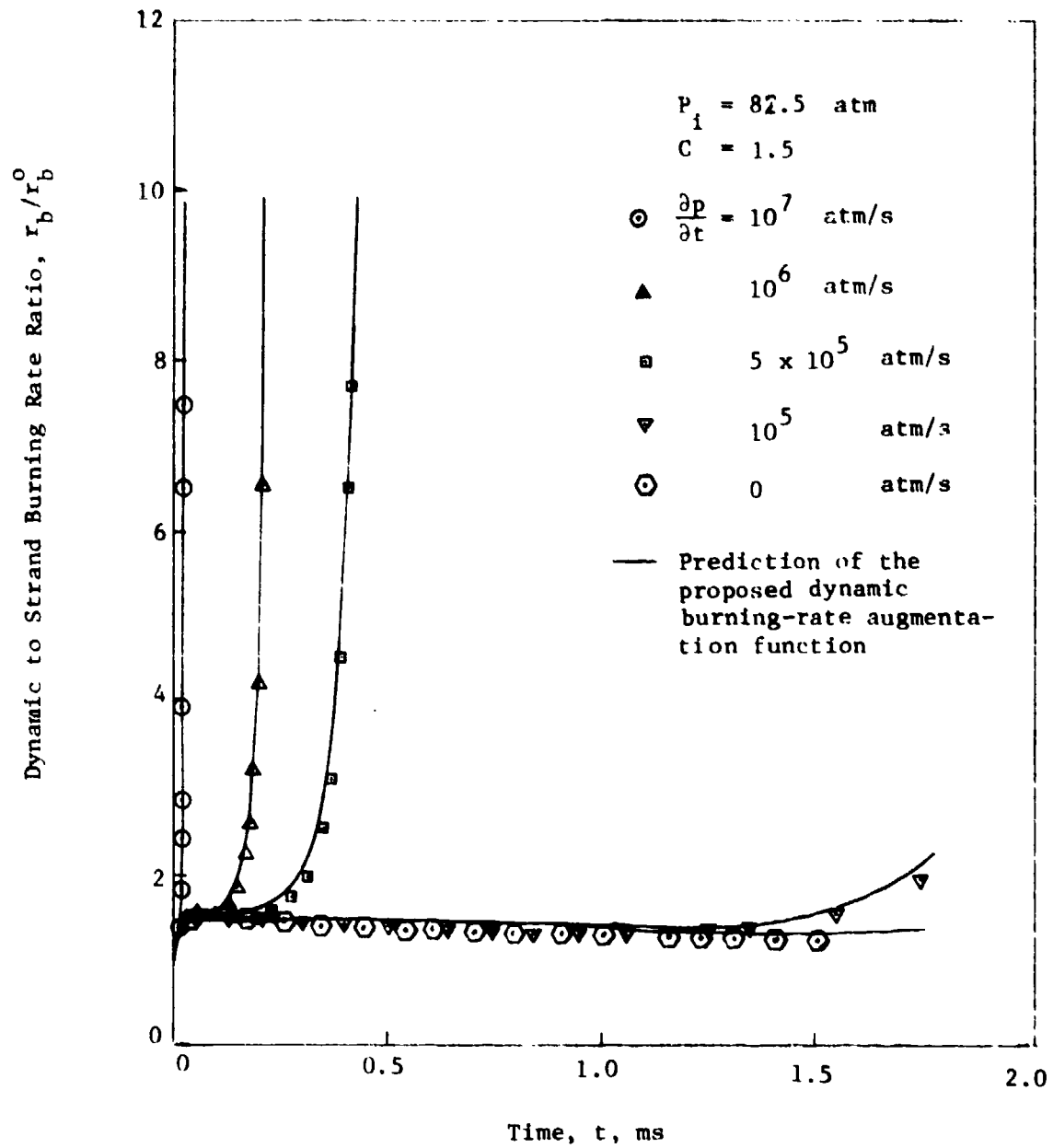


Fig. 11 Comparison of the dynamic burning rate data with the prediction from burning rate augmentation function

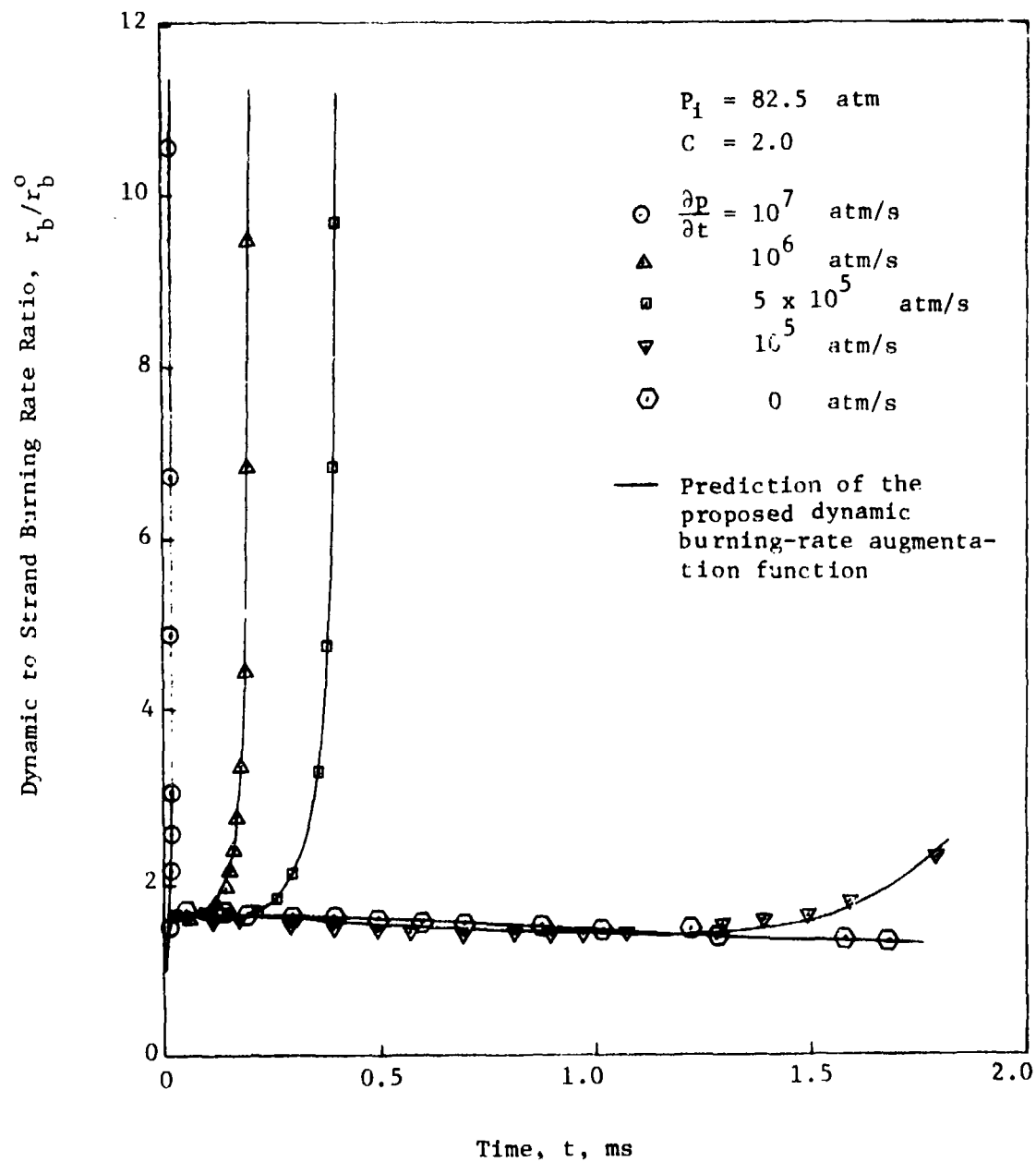


Fig. 12 Comparison of the dynamic burning rate data with the prediction from burning rate augmentation function

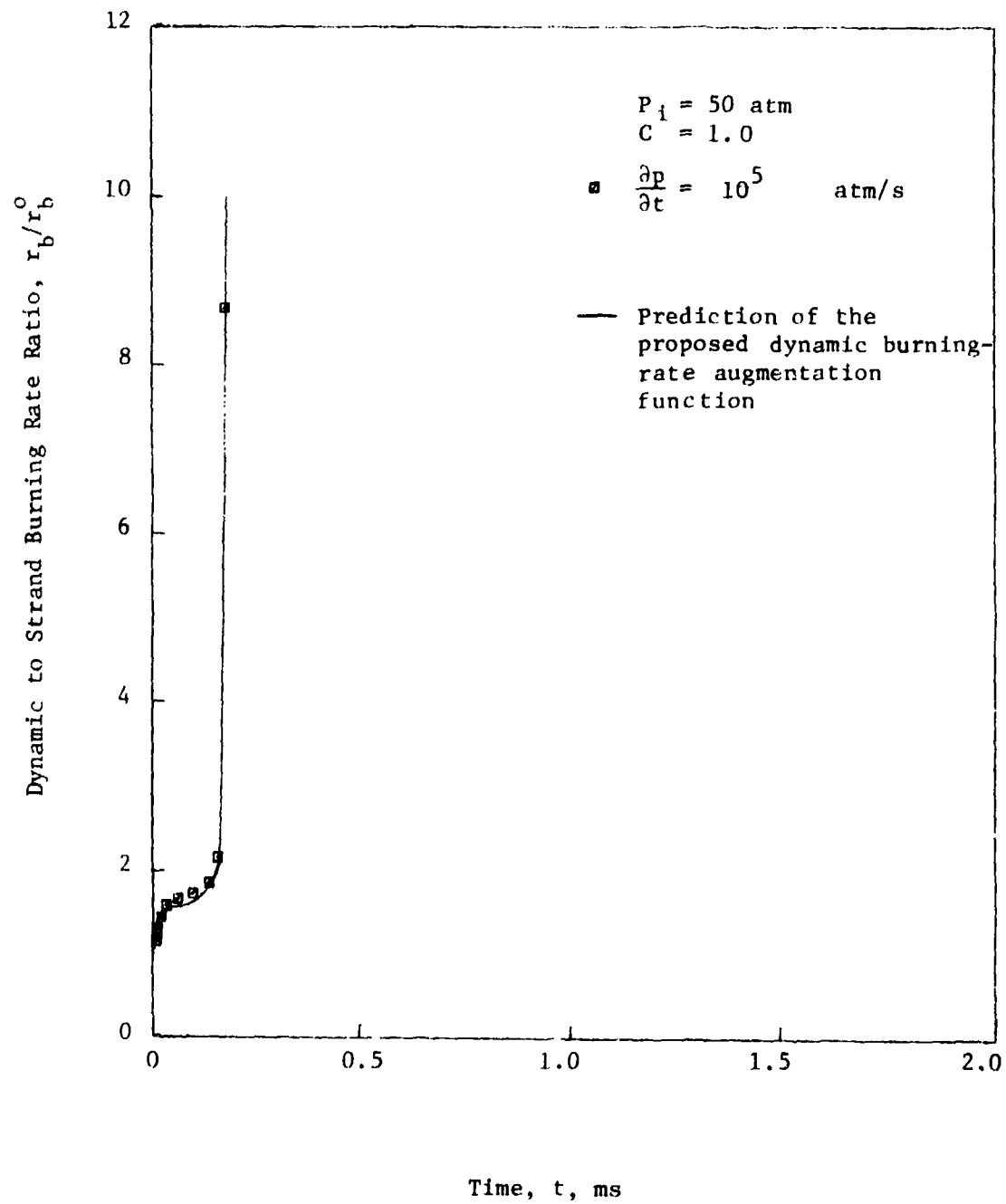


Fig. 13 Comparison of the dynamic burning rate data with the prediction from burning rate augmentation function

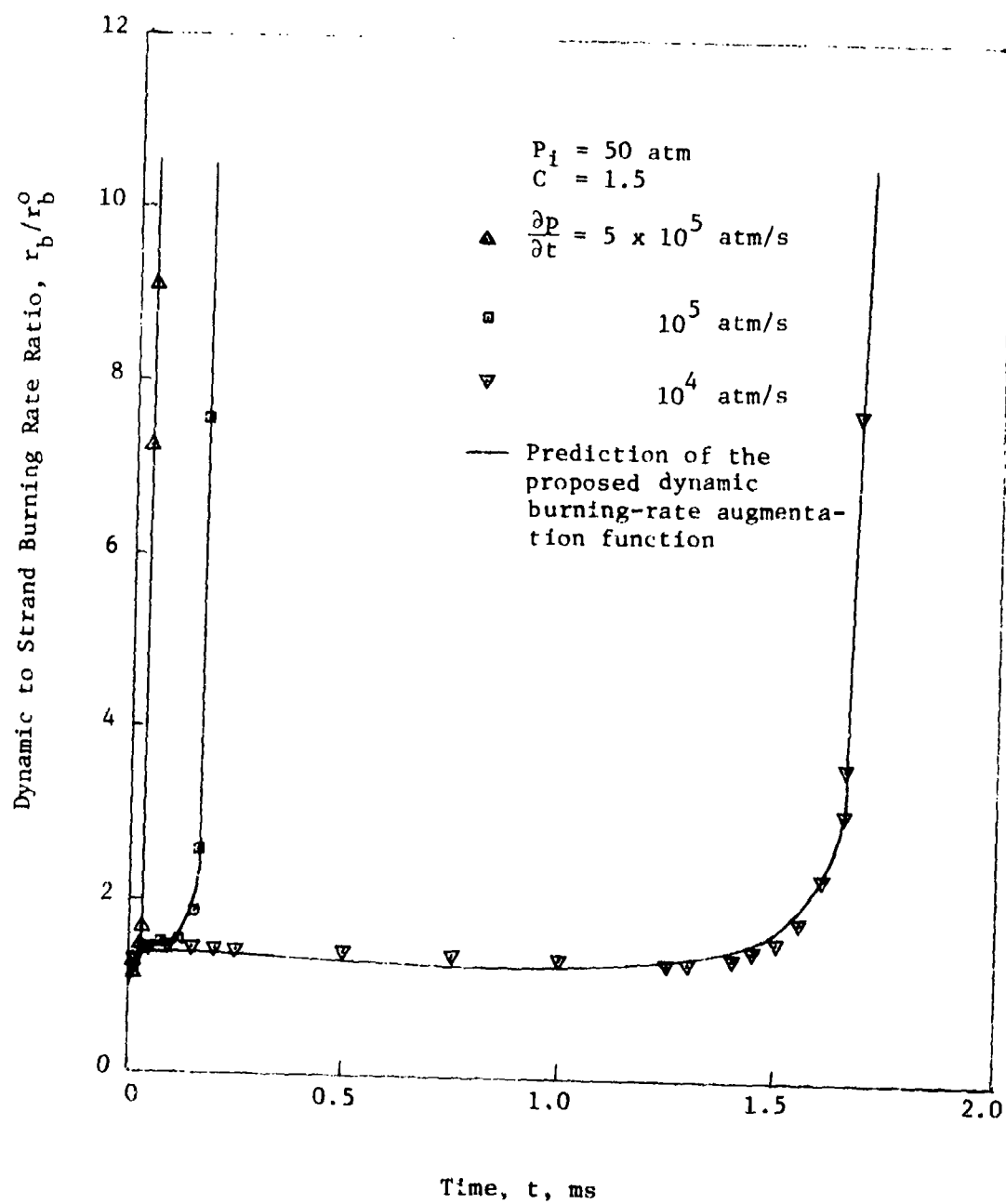


Fig.14 Comparison of the dynamic burning rate data with the prediction from burning rate augmentation function

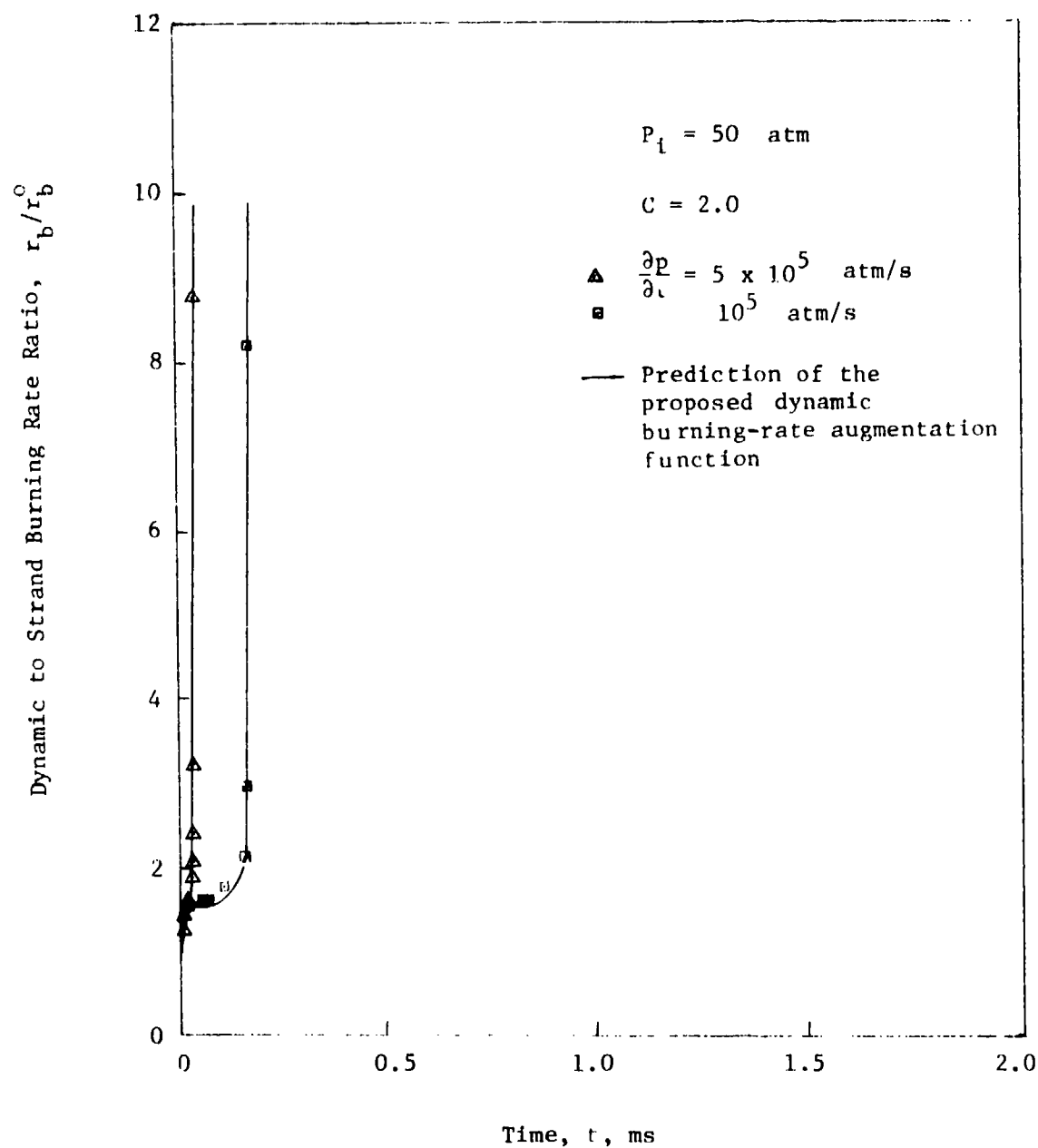


Fig. 15 Comparison of the dynamic burning rate data with the prediction from burning rate augmentation function

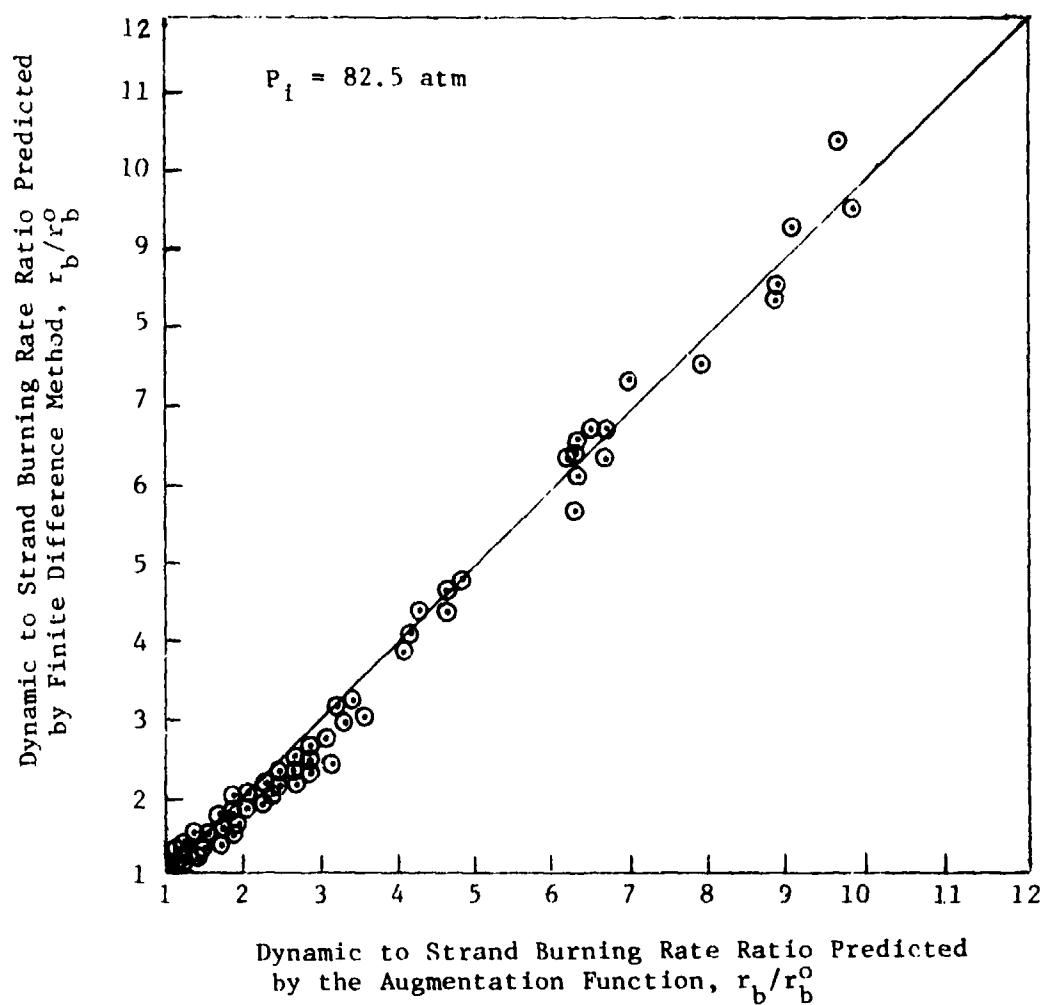


Fig. 16 Comparison of the dynamic burning rates calculated by two different methods

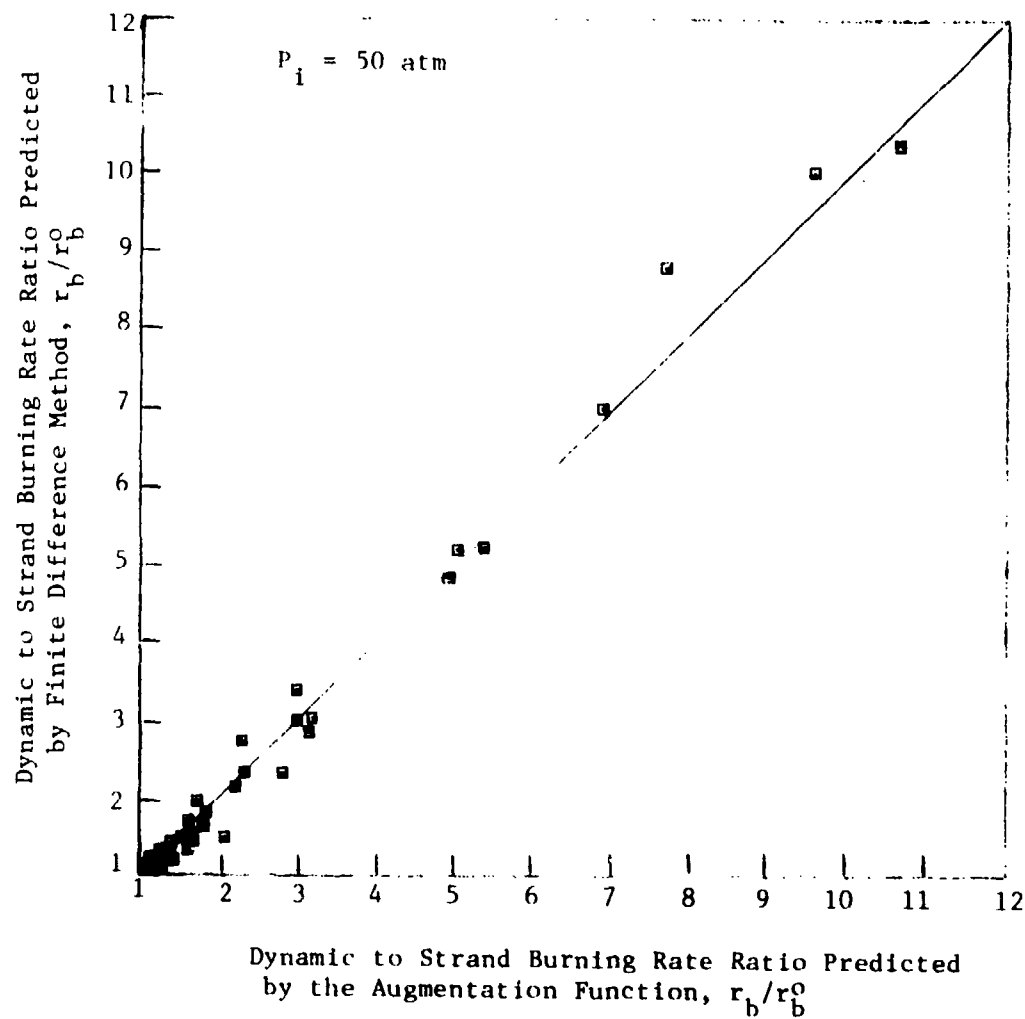


Fig. 17 Comparison of the dynamic burning rates calculated by two different methods

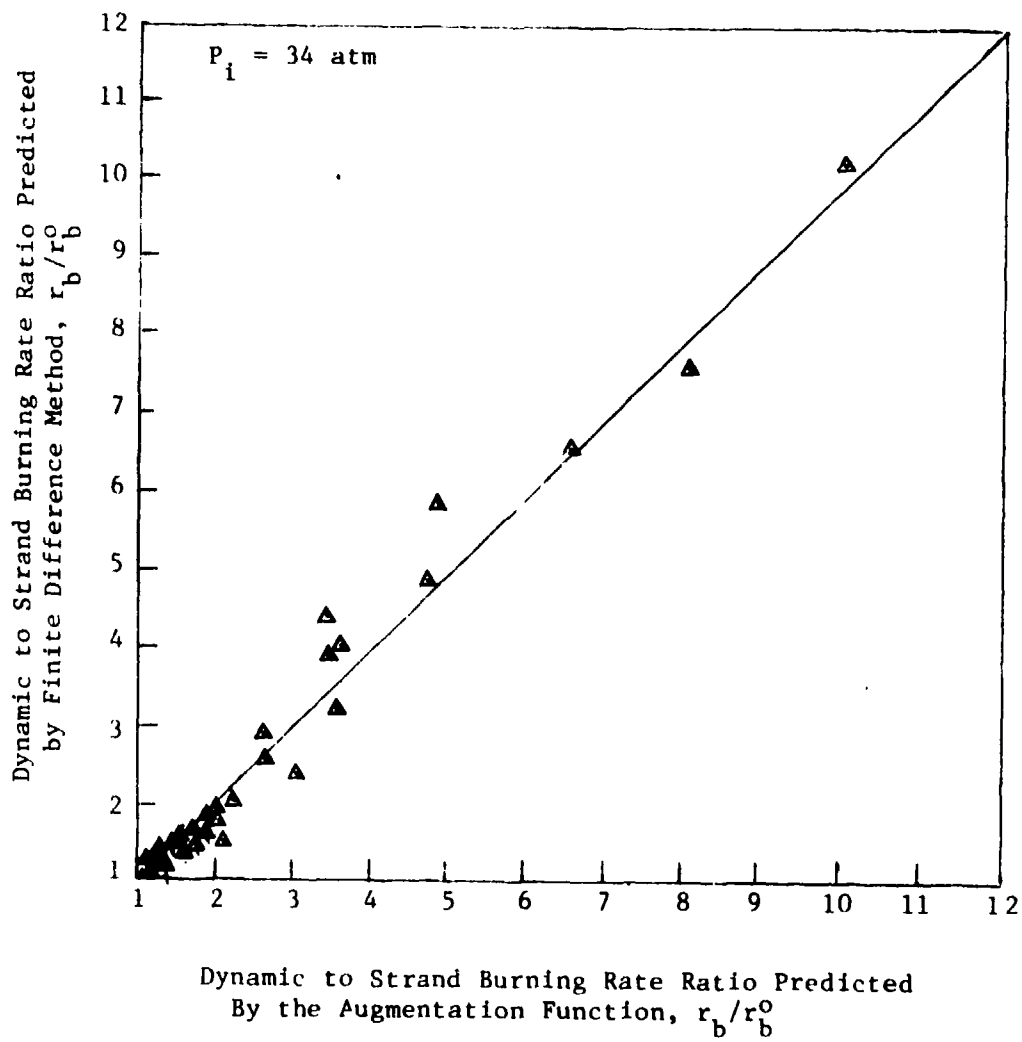


Fig. 18 Comparison of the dynamic burning rates calculated by two different methods

- (a) The pressurization rate was assumed to be constant for the entire period.
- (b) In the generation of augmentation function, no pressure cutoff was considered.
- (c) The initial propellant subsurface temperature profile was approximated by an exponential function. This may not always be an accurate representation of the actual temperature profile.
- (d) The function should not be used for cases with $C < 1$.
- (e) The Zeldovich method, which was used to calculate the dynamic burning rate, breaks down under erosive burning conditions. Therefore, the proposed function should not be used for situations involving erosive burning.

2.2 Technological Gaps in the Existing Granular Bed Combustion Models for DDT Studies

In recent years, four one-dimensional two-phase combustion models⁸⁻¹² have been developed for prediction of the combustion processes in granular propellant beds. These models were independently developed at The Pennsylvania State University, Gough Associates, Inc., The University of Illinois, and Calspan Corp. for interior ballistic predictions. They were reviewed and summarized in a JANNAF Workshop⁶ conducted three years ago.

Some modifications and improvements in these models have been made since the JANNAF Workshop. At the Pennsylvania State University, improvements have been made in the following three areas. The intragranular stress and particle-wall friction measurements in granular bed were made and correlations were obtained.¹³ The speed of sound transmitted through a packed granular bed as a function of porosity was also obtained. To determine the actual flow rates from percussion primers, a primer characterization study was conducted. The results of this study¹⁴ were used as input data for granular bed combustion calculations. The boundary condition treatment at the ends of the granular bed has been further improved. The most up-to-date procedures for boundary condition calculations are reported in Ref. 15. The comparison of theoretical predictions and experimental data are given in Refs. 15 and 16.

The flow resistance measurements through granular propellant beds made of cylindrical grains were conducted by Robbins and Gough¹⁷ and their latest experimental results are in close agreement with Kuo-Nydegger's correlation.¹⁸ For large caliber systems, the multi-dimensional effect is important, and Gough has recently developed a two-dimensional convective flame spreading model.¹⁹ Special emphases were placed in the description of the internal boundaries so that the effect of bag material, liners and additives can be studied.

Krier²⁰ has changed his earlier continuum mechanics model¹¹ into a separated two-phase flow model²⁰ for studying DDT phenomena in granular propellant beds. A number of empirical correlations were altered for using them beyond the ranges for which these correlations were developed. The lack of suitable constitutive relationships were noted.

Besides the constitutive relationships for flow resistance, heat transfer, intragranular stress, etc., there are a number of technological gaps that should be narrowed in order to extend the existing granular bed combustion models for DDT studies. These are given in the following.

1. Better ignition criterion has to be established. The gasification of reactive species may not result in an instantaneous reaction to generate heat at the location of gasification. Also, the products in the form of condensed phases may have non-negligible effect on ignition. The effect of shock wave propagation in granular material can also have important contribution to ignition. The shear, compression, and friction effects should also be considered.
2. The evaluation of intragranular stresses transmitted through aggregates of solid propellants under dynamic conditions must be performed.
3. The fracture of grains and resulting increase in the specific surface area of the propellant under dynamic compression should be studied.
4. Dynamic and erosive burning effects during the transition process from deflagration to detonation should also be evaluated.

5. The treatment of extremely steep pressure gradients near the wave front in the granular bed should be incorporated in the solution scheme.
6. Understanding of the generation of hot spots in solid propellants must be advanced.
7. Mechanical properties and fracture behavior of the propellant under extremely rapid pressurization conditions must be characterized.

2.3 Documentation of the Fixed and Mobile Granular Bed Combustion Codes (MGBC and FGBC)

To facilitate the use and understanding of the granular bed combustion program, two user's manuals were prepared: one was designed for mobile granular bed combustion²¹ and the other for fixed granular bed combustion.²² These manuals outline theoretical models, numerical solution methods, and use of computer codes for predicting the physical processes involved in mobile and fixed granular bed combustion of solid propellants, respectively. The manuals provide details of the following: (1) description of the physical processes; (2) basic assumptions used in the model; (3) formulation of the model, using the basic conservation equations for single or two-phase flow; (4) initial and boundary conditions; (5) use of method of characteristics for extraneous boundary conditions; (6) procedures for the propellant surface temperature calculations; (7) empirical correlations used in the model; (8) numerical scheme for the interior points; (9) numerical scheme for the boundary conditions; (10) description of the main program and the subroutines; (11) input data for the initial and restart runs; (12) typical input and output of the program; (13) finite-difference equations for the governing equations; (14) procedures for determining the flow properties at the boundaries of the granular bed; and (15) glossary of important variables used in the program. Both the MGBC manual (78 pages) and the FGBC manual (40 pages) have been delivered to NWC for use by NWC personnel. It is believed the manuals give sufficient details to enable users to easily modify the program for particular applications.

2.4 Delivery of MGBC and FGBC Programs to NWC and Consultation for Their Implementation

Both MGBC and FGBC programs were delivered to NWC during the early phase of the contract period. Before delivery, the programs were revised by deleting unnecessary portions and by adding a large number of comment cards to facilitate understanding of the program by new users.

MGBC was delivered in the form of a magnetic tape, and FGBC was delivered in the form of cards. Sample case input data and output listings were also prepared and delivered with each source program. An updated version of the MGBC program was mailed to Mr. C. F. Price in September 1979. Two sets of sample data with the description of Input Format were prepared for the updated MGBC.

During the contract period, consultations were provided for implementation of these programs onto the computer at NWC. These programs have been successfully executed after some modifications by MR. C. F. Price at MWC.

III. SUMMARY AND CONCLUSIONS

1. Dynamic burning effects in the combustion of solid propellant cracks were studied, using the Zeldovich quasi-steady flame approach.
2. Transient heat conduction equation for the solid propellant was solved with the given Zeldovich burning rate map by using an implicit finite difference numerical scheme.
3. Computed results indicate that the dynamic burning effect becomes stronger for higher pressurization rates, higher initial energy storage in the solid propellant (i.e., thicker temperature profile at the onset of ablation), and lower initial pressure.
4. For monotonically increasing pressure with a constant pressurization rate, a runaway condition for the dynamic burning rate was observed. The time required to reach the runaway condition decreases as the pressurization rate is increased, or when the initial pressure is decreased; the runaway time is found to be very weakly dependent upon the initial propellant temperature profiles considered in this study.
5. The dynamic burning effect was found to be important in the combustion processes in solid propellant cracks. The dynamic burning consideration was incorporated into the crack combustion code (CCC) in two ways. The first method, which involves a direct coupling of the dynamic burning subroutine with CCC, requires extremely small time increments and was, therefore, not used. The second method involves the development of a dynamic burning-rate augmentation function for an indirect coupling with CCC.
6. A dynamic burning-rate augmentation function was generated. This function fits the burning rate data, calculated from the Zeldovich method, over a broad range of conditions. The augmentation function was incorporated into CCC.

7. A literature survey was conducted on recent studies in granular propellant bed combustion in order to examine their applicability for DDT studies. Technological gaps in the existing granular bed combustion models for DDT study were listed.
8. Two user's manuals were prepared and delivered to NWC. One was designed for mobile granular bed combustion (MGBC) and the other for fixed granular bed combustion (FGBC).
9. The updated computer codes for MGBC and FGBC were also delivered to NWC.

IV. REFERENCES

1. Kuo, K.K., and Coates, G.R., "Review of Dynamic Burning of Solid Propellants in Gun and Rocket Propulsion Systems," the Sixteenth Symposium (International) on Combustion, MIT, Cambridge, Massachusetts, pp. 1177-1192, August, 1976.
2. Summerfield, M., Cavney, L.H., Battista, R.A., Kubota, N., and Isoda, H., "Theory of Dynamic Extinguishment of Solid Propellants with Special Reference to Nonsteady Feedback Law," Journal of Spacecraft and Rockets, Vol. 8, No. 3, pp. 551-558, March, 1971.
3. Kuo, K.K., Chen, A.T., and Davis, T.R., "Convective Burning in Solid-Propellant Cracks," AIAA Journal, Vol. 16, No. 6, pp. 600-607, June, 1978.
4. Kuo, K.K., McClure, D.R., Chen, A.T., and Lucas, F.G., "Transient Combustion in Solid Propellant Cracks," Naval Weapons Center Report No. NWC TP 5943, October, 1977.
5. Kuo, K.K., Kovalcin, R.L., and Ackman, S.J., "Convective Burning in Isolated Solid-Propellant Cracks," Annual Report to Naval Weapons Center, February, 1978.
6. Kuo, K.K., "A Summary of the JANNAF Workshop on Theoretical Modelling and Experimental Measurements of the Combustion and Fluid Flow Processes in Gun Propellant Charges," 13th JANNAF Combustion Meeting, CPIA Publication 281, Vol. 1, pp. 213-233, September, 1976.
7. Barr, A.J., Goodnight, J.H., Sall, J.P., and Helwig, J.T., "Statistical Analysis Systems," SAS Institute, Inc., 1976.

8. Kuo, K.K., Koo, J.H., Davis, T.R., and Coates, G.R., "Transient Combustion in Mobile Gas-Permeable Propellants," Acta Astronautica, Vol. 3., No.7-8, pp. 574-591, July, 1976.
9. Gough, P.S., "Fundamental Investigation of the Interior Ballistics of Guns," Final Report, Contract N00174-73-C-0501, SCR-R-75, July, 1974.
10. Gough, P.S., "The Flow of a Compressible Gas Through an Aggregate of Mobile Reacting Particles," Ph.D. Thesis, McGill University, December, 1974.
11. Krier, H., and Rajan, S., "Flame Spreading and Combustion in Packed Beds of Propellant Grains," AIAA Paper 75-240, AIAA 13th Aerospace Sciences Meeting, January, 1975.
12. Fisher, E.B., and Trippe, A.P., "Mathematical Model of Center Core Ignition in the 175 mm Gun," Calspan Report No. VQ-5163-D-2, March, 1974.
13. Kuo, K.K., Moore, B.B., and Yang, V., "Measurements and Correlation of Intragranular Stress and Particle-Wall Friction in Granular Propellant Beds," 16th JANNAF Combustion Meeting, Naval Postgraduate School, Monterey, California, September, 1979.
14. Kuo, K.K., Moore, B.B., and Chen, D.Y., "Characterization of Mass Flow Rates for Various Percussion Primers," 7th International Colloquium on Gasdynamics of Explosives and Reactive Systems, Gottingen, West Germany, August, 1979.
15. Chen, D.Y., and Kuo, K.K., "Boundary Condition Treatment of Transient Two-Phase Flows in Gun Systems," AIAA Paper No. 80-0080, to be presented at Pasadena, California, January, 1980.

16. Davis, T.R., and Kuo, K.K., "Experimental Study of the Combustion Process in Granular Propellant Beds," Journal of Spacecraft and Rockets, Vol. 16, No. 4, pp. 203-209, July-August, 1979.
17. Robbins, F., and Gough, P.S., "Influence of Length and Diameter of Cylinders on Packed Bed Flow Resistance," 16th JANNAF Combustion Meeting, Naval Postgraduate School, Monterey, California, September, 1979.
18. Kuo, K.K., and Nydegger, C.C., "Flow Resistance Measurement and Correlation in a Packed Bed of WC 870 Ball Propellants," Journal of Ballistics, Vol.2, No. 1, pp. 1-26, 1978.
19. Gough, P.S., "Two Dimensional Convective Flamespreading in Packed Beds of Granular Propellant," Contract Report ARBRL-CR-00404, July, 1979.
20. Krier, H., and Kezerle, J.A., "A Separated Two-Phase Flow Analysis to Study Deflagration-to-Detonation Transition (DDT) in Granulated Propellant," Seventeenth Symposium (International) on Combustion, pp. 23-34, 1978.
21. Kuo, K.K., and Kumar, M., "Program Description Manual for Mobile Granular Bed Combustion (MGBC) Code," Submitted to NWC, China Lake, California, January, 1979, (78 pages).
22. Kuo, K.K., Kuo, O.J., and Kumar, M., "Program Description Manual for Fixed Granular Bed Combustion (FGBC) Code," Submitted to NWC, China Lake, California, March, 1979, (40 pages).

APPENDIX I

STEADY STATE BURNING DATA FOR PROPELLANT A

Burning Rate (cm/s) of Propellant A as a function
of pressure and initial temperature

Initial Temp., K	Pressure, g_f/cm^2				
	15,470	36,910	72,770	107,900	143,400
274.7	0.467	0.711	0.960	1.143	1.229
294.1	0.488	0.729	0.983	1.179	1.252
321.9	0.516	0.759	1.029	1.234	1.306

Surface temperature at Ignition (K) of Propellant A
as a function of pressure and initial temperature

Initial Temp., K	Pressure, g_f/cm^2				
	15,470	36,910	72,770	107,900	143,400
274.7	773.278	788.155	799.150	805.678	808.423
294.1	774.809	789.069	800.030	806.850	809.128
321.9	776.761	790.5295	801.734	808.578	810.738

NWC TP 6193
APPENDIX II

INPUT DATA DESCRIPTION FOR DYNAMIC BURNING RATE PROGRAM

<u>Computer Symbol</u>	<u>Symbol in Analysis</u>	<u>Description</u>	<u>Units</u>
<u>Card 1 (5D14.7)</u>			
SAENG	E_a	Surface activation energy used in: $r_b = A_s \exp(-E_a / R_u T_{ps})$	cal/g-mol
ARRHC	A_s	Arrhenius coefficient	cm/s
WTF		Weight fraction in calculating new assumed r_b . $0 < WTF \leq 1$	
PDYMAX		Maximum pressure above which no dynamic burning effect is considered	g/cm^2
PRATE	$\frac{dP}{dt}$	The ramp pressurization rate	$\text{g/cm}^2\text{-s}$
<u>Card 2 (5D12.5)</u>			
DELTAT	t	Time increment	s
ALPHAP	α_p	Thermal diffusivity	cm^2/s
BREXP	n	Burning rate exponent in Saint-Robert's Law	
A	a	Burning rate coefficient in Saint-Robert's Law	$(\text{cm/s})/(\text{g/cm}^2)^n$
YTPDIP	$(y_{T_p})_{\text{dip}}$	The depth below the burning propellant surface at which the dipstick ignition criterion is applied.	cm
<u>Card 3 (2D12.5, 1X, 815)</u>			
TPI	T_{P_i}	Propellant initial temperature	K
FAC	FAC	Factor used in the expansion of the grid size normal to the burning surface $\Delta y(I) = (1 + \text{FAC})\Delta y(I-1)$	
KX		The integer to designate the axial location along the crack. KX=1 represents the crack entrance mesh point; KX=NMAX+1 represents the closed end of the crack.	
NMAX		The total number of Δx intervals along the crack.	

<u>Computer Symbol</u>	<u>Symbol in Analysis</u>	<u>Description</u>	<u>Units</u>
<u>Card 3 (2D12.5, 1X, 815) (con't)</u>			
ITRMAX		The maximum number of iterations allowed for the convergence of burning rate.	
NDTMAX		The maximum number of Δt in an initial or restart run.	
IRSTRT		The flag to indicate the restart run. IRSTRT=1, for restart run IRSTRT=0, for initial run	
NPRINT		The flat to control the printing of output. Print after every NPRINT* Δt .	
IØVRWT		A flat to control the overwrite option of the subsurface temperature profile. IØVRWT \neq 0, an exponential temperature profile is used to overwrite the initial temperature profile.	
NEXTIN		A flag to control the burning rate to avoid extinction. NEXTIN \neq 0, instantaneous burning rate cannot be less than the steady-state value.	
<u>Card 4 (5D12.5)</u>			
CTS1	C_{TS_1}	Coefficient 1 used in the temperature sensitivity expression: $\sigma_p = C_{TS_1} + C_{TS_2} P$	1/K
CTS2	C_{TS_2}	Coefficient 2 used in the temperature sensitivity expression: $\sigma_p = C_{TS_1} + C_{TS_2} P$	cm ² /g-K
TREFL	T_{ref}	The lowest available T_{p_i} data used as a reference temperature for the equivalent T_{p_i} through the use of temperature sensitivity.	K

<u>Computer Symbol</u>	<u>Symbol in Analysis</u>	<u>Description</u>	<u>Units</u>
<u>Card 4 (5D12.5)(Con't)</u>			
WTFG		Weighting factor for the temperature gradient at the propellant surface. $0 < \text{WTFG} \leq 1$. $\phi(\text{ITER}+1) = (1-\text{WTFG})\phi_{\text{QSF}} + \text{WTFG}*\phi(\text{ITER})$	
SLØPC	S_c	The slope constant in the exponential distribution of the temperature profile (which is used to approximate any sub-surface profile).	
$\frac{T_p - T_{p_i}}{T_{ps} - T_{pi}} = e^{-\frac{r_b y}{\alpha_p S_c}}$			
<u>Card 5 (2D12.5, I4)</u>			
Time	t	Time at beginning of a run	s
PP	P	The initial pressure used in restart run.	g/cm^2
NDT		The number of Δt at the restart.	
<u>Card 6a and b (19A4)</u>			
TP(KX,J)	T_p	The subsurface temperature profile for 38 mesh points at the beginning of each run.	
<u>Card 7 (2I10)</u>			
IRØW		The number of isobaric lines in the $r_{b\text{tab}}(T_{p_i\text{tab}}, P_{\text{tab}})$ input map.	
INØ		The number of data points on each isobaric line.	
<u>Card 8 a - d (6D12.5)</u>			
PTBL	P_{tab}	Tabulated pressures in the table.	g/cm^2

<u>Computer Symbol</u>	<u>Symbol in Analysis</u>	<u>Description</u>	<u>Units</u>
<u>Card 9 (6D12.5)*</u>			
BRGIV	$r_{b_{tab}}$	Tabulated burning rate $r_{b_{tab}}(T_{p_{i_{tab}}}, P_{tab})$	cm/s
<u>Card 10 (6D12.5)*</u>			
PHIGIV	$T_{p_{i_{tab}}}$	Tabulated initial propellant temperature.	K
<u>Card 11 (4D10.4)</u>			
P	P	Initial pressure at t=0.	g/cm^2
TPSCRI	$T_{ps_{cri}}$	The critical surface temperature, below which there is no burning.	K
TPSINI	$T_{ps_{initial}}$	Initial propellant surface temperature	K
<u>Card 12 (D10.4)</u>			
TLRNSM		Maximum tolerance for the convergence of burning rate.	

* Card 9 and 10 are alternately repeated IRØW times.

NWC TP 6193
INITIAL DISTRIBUTION

1 Director of Navy Laboratories
8 Naval Air Systems Command
 AIR-30212 (2)
 AIR-330 (1)
 AIR-330B, Robert H. Heitkotter (1)
 AIR-330D (1)
 AIR-536 (1)
 AIR-950D (2)
4 Chief of Naval Operations
2 Chief of Naval Material
 MAT-03 (1)
 MAT-03PB (1)
6 Naval Sea Systems Command
 SEA-003 (1)
 SEA-62R2, Murrin (1)
 SEA-62R22, Cassel (1)
 SEA-9961 (1)
 SEA-99612 (2)
7 Chief of Naval Research, Arlington
 ONR-100 (1)
 ONR-102 (1)
 ONR-4C1 (1)
 ONR-420 (1)
 ONR-472 (1)
 ONR-473
 Richard Miller (1)
 James R. Patton, Jr. (1)
3 Naval Ordnance Station, Indian Head
 Code 525, Peter Stang (1)
 Code 5252H, V. Ezerins (1)
 Technical Library (1)
3 Naval Postgraduate School, Monterey
 Code 57, Fuhs (1)
 Code 57NT, Netzer (1)
 Technical Library (1)
3 Naval Research Laboratory
 Code 2021 (1)
 Code 6130, Chemistry Division (1)
 Technical Library (1)
2 Naval Surface Weapons Center Detachment, White Oak Laboratory,
 Silver Spring
 Code 240, Sigmund Jacobs (1)
 G. B. Wilmot (1)
1 Naval Underwater Systems Center, Newport (Code 5B331, Robert S. Lazar)
1 Naval Weapons Evaluation Facility, Kirtland Air Force Base (Code 401)
2 Navy Strategic Systems Project Office
 SP-2731, Roy Kinert (1)
 NSP-2731, Throckmorton (1)

- 2 Army Armament Research and Development Command, Dover
 - DRDAR-SCA-PE, L. Stiefel (1)
 - LCWSL, C. Lenchitz (1)
- 1 Army Missile Research & Development Command, Redstone Arsenal
 - (DRMI-RK, Dr. R. G. Rhoades)
- 1 Army Armament Research & Development Center (SMUPA-TS-TS, J. Picard)
- 3 Army Ballistic Research Laboratories, Aberdeen Proving Ground
 - DRDAR-BLP
 - Austin W. Barrows (1)
 - Ingo W. May (1)
 - DRDAR-TSB-S (STINFO) (1)
- 1 Rock Island Arsenal (Edward Haug)
- 1 Air Force Armament Laboratory, Eglin Air Force Base (DLDL, Otto K. Heiney)
- 3 Air Force Rocket Propulsion Laboratory, Edwards Air Force Base
 - DYSC, Wilbur C. Andrepont (1)
 - Robert Geisler (1)
 - Dr. R. Weiss (1)
- 2 Air Force Office of Scientific Research
 - Capt. R. F. Sperlein (1)
 - Bernard T. Wolfson (1)
- 12 Defense Technical Information Center
 - 1 National Aeronautics & Space Administration (Code RP, Frank W. Stephenson, Jr.)
 - 2 George C. Marshall Space Flight Center
 - SE-ASTN-PEA, John Q. Miller (1)
 - Richard J. Richmond (1)
 - 1 Lewis Research Center (Richard J. Priem)
 - 1 Lyndon B. Johnson Space Center (EP, Joseph G. Thibodaux)
 - 1 Aerojet Solid Propulsion Company, Sacramento, CA (Dept 4350, M. Ditore) via AFPRO
 - 1 Aeronautical Research Associates of Princeton, Inc., Princeton, NJ (E. S. Fishburne)
 - 1 Aerospace Corporation, Los Angeles, CA (Ellis M. Landsbaum)
 - 1 Allegany Ballistics Laboratory, Cumberland, MD (Roy R. Miller)
 - 1 Atlantic Research Corporation, Alexandria, VA (Merrill K. King)
 - 1 Battelle Memorial Institute, Columbus, OH (Abbott A. Putman)
 - 1 Brigham Young University, Provo, UT (673/WldB, M. Beckstead)
 - 1 California State University Sacramento, Sacramento, CA
 - (School of Engineering, Frederick H. Reardon)
 - 1 Calspan Corporation, Buffalo, NY (Edward B. Fisher)
 - 1 Chemical Propulsion Information Agency, Applied Physics Laboratory, Laurel, MD (Thomas W. Christian)
 - 3 Georgia Institute of Technology, Atlanta, GA
 - Ben T. Zinn (1)
 - Edward W. Price (1)
 - Warren C. Strahle (1)
 - 1 General Applied Science Laboratory, Westbury Long Island, NY
 - (John Erdos)

- 1 General Dynamics Corporation, Pomona Division, Pomona, CA
(Paul L. Boettcher)
- 2 Hercules Incorporated, Bacchus Works, Magna, UT
Ken McCarty (1)
Ronald L. Simmons (1)
- 1 Hercules, Incorporated, McGregor, TX (William G. Haynes)
- 1 Institute for Defense Analyses, Arlington, VA (R. C. Oliver)
- 2 Jet Propulsion Laboratory, Pasadena, CA
Fred E. C. Culick (1)
Leon D. Strand (1)
- 2 Lockheed Missiles and Space Company, Sunnyvale, CA
J. Linsk (1)
- 3 Lockheed Palo Alto Research Laboratory
R. Byrd (1)
G. Lo (1)
H. Marshall (1)
- 1 Pennsylvania State University, State College, PA (Applied
Research Lab., Gerard M. Faeth)
- 2 Princeton University Forrestal Campus Library, Princeton, NJ
Leonard H. Caveny (1)
W. Sirignano (1)
- 1 Purdue University, West Lafayette, IN (School of Mechanical
Engineering, John R. Osborn)
- 1 Rockwell International Corporation, Canoga Park, CA (BA08, Joseph
E. Flanagan)
- 1 Science Applications, Inc., Woodland Hills, CA (R. B. Edelman/Suite 423)
- 1 Southwest Research Institute, San Antonio, TX (Fire Research
Section, William H. McLain)
- 1 TRW Systems, Inc., Redondo Beach, CA (A. C. Ellings)
- 1 Thiokol Corporation, Huntsville Division, Huntsville, AL
(David A. Flanagan)
- 1 Thiokol Corporation, Wasatch Division, Brigham City, UT
(Steve Polkman)
- 1 United Technologies Corporation, East Hartford, CT (R. H. W. Woesche)
- 1 United Technologies Corporation, Sunnyvale, CA (Chemical
Systems Division, Robert S. Brown)
- 1 Universal Propulsion Co., Riverside, CA (H. J. McSpadden)
- 1 University of California, San Diego, La Jolla, CA (AMES Dept,
Forman A. Williams)
- 1 University of Illinois, Urbana, IL (AAE Dept., Herman Krier)
- 1 University of Southern California, Los Angeles, CA (Mechanical
Engineering Dept/OHE200, M. Gerstein)
- 2 University of Utah, Salt Lake City, UT
Dept of Chemical Engineering, Alva D. Baer (1)
G. A. Flandro (1)
- 2 Whittaker Corporation, Berrite Division, Saugus, CA
L. Bloom (1)
L. LoFiego (1)
- 1 University of Waterloo, Ontario, Canada (Department of Mechanical
Engineering, Clarke E. Hermance) via Naval Air Systems Command
(AIR-C9C2)